UNIVERSITAT AUTÒNOMA DE BARCELONA
GRUP DE FÍSICA DE LES RADIACIONS

A journey of Ultra Heavy Cosmic Ray Nuclei with $Z \gtrsim 65$: From their detection at the Earth neighborhood back to their nucleosynthesis sites.

Joan Font i Serra

PhD Thesis

July 2004

To my parents, Joan and Montserrat,

whose patience and support are unlimitted

Acknowledgements

Under standard conditions, it would be really easy to find a more or less extensive set of persons to whom give my acknowledgments, but the different situations with which I encountered, have significantlly reduced the list. I do not mean the trip that I have run for the realisation of this work would be comparable to the troubled journey of Ulysses across the garden of Poseidon, but in specific moments it seemed a reduced version of an adventure written by Homer himself.

Nevertheless, according to the ideas of Nietzche about the difficulties found during life, there must be pain, anguish, envy and humiliation in all profound changes that one decides to do. This reasoning offers an excellent consolation to my particular Odyssey.

In any case, I would like to mention the following persons without whose intervention, this thesis could not be finished:

I thank Dr. Carles Domingo for his guidance and constant support. He has been an outstanding thesis adviser and has offered enough freedom of motion for the realisation of this work. Since this work has been written, it must contain obscurities and mistakes, there are fewer of them because of his suggestions.

I express my gratitude to professor F. Fernández for accepting to develop my research task in the Grup de Física de les Radiacions.

I also want to thank professor C. Baixeras for her comments on specific aspects of this work. I also would like to extend my acknowledgement to the rest of colleagues in our group for their help on different drawbacks found during the realisation of the present work. Among them, I'd like to point up Dr. K. Amgarou who has offered me his unconditional help and support in all stages of this work providing software solutions and clever comments, always with a good sense of humour.

I wish to thank Mercè Compte and Marisa Mas (microscopists in Universitat Autònoma de Barcelona) for their care in locating and measuring the geometry of the registered tracks and for their virtually infinite patience when they had to relocate and to remeasure events.

Finally, I want to include in this list of essential persons, my parents and sisters for their patience, care and in some cases financial support. I cannot forget to mention my friends of mind, Enric, Josep, Santi and Olga with who I've shared more than extensive conversations about this work and other topics of knowledge. They always have shown a surprising interest for my work and have encouraged me to write it down.

Contents

List of Figures

List of Tables

List of abreviations

ACCESS, Advanced Cosmic-ray Composition Experiment for the Space Station.
AGB, Assymptotic Giantr Branch.
CRIS, Cosmic Ray Isotope Spectrometer.
EAS, Extensive Air Showers.
ESA, European Space Agency
ESTEC, European Space Research and Technology Center.
FD, Fractional Difference.
FIP, Fisrt Ionisation Potential.
GCRS, Galactic Cosmic Ray Source.
GFR, Grup de Física de les Radiacions.
HEAO, High Energy Astronomy Observatory.
HDM, Halo Difussion Model.
HNE, Heavy Nuclei Experiment.
HRD, Herzprung-Russell Diagram.
ISM, Interstelllar Medium.
LBM, Leaky Box Model.
LDEF, Long Duration Exposure Facility.
LTI, Latent Track Intensification.
MREL, Modified Restricted Energy Loss.
NASA, National Aeronautincs and Space Administration.
PCR, Primary Csmic Rays.
PLD, Path Leangth Distribution.
REL, Restricted Energy Loss.
RERFG, Restricted Etch Rate Fractional Gradient.
RGB, Red Giant Branch.
RTE, Registration Temperature Effect.
SSNTD, Solid State Nuclear Track Detector.
S_n, Neutron separation energy.
SN, SuperNova
SNII, SuperNova of type II.
SNR, SuperNova Remnant.
SS, Solar System.
SS_0, Solar System as source abundances.
SS_P, Propagated Solar System abundances.
TIGER, Trans-Iron Galactic Element Recorder.

UHCR, Ultra Heavy Cosmic Rays.
UHCRE, Ultra Heavy Cosmic Rays Experiment.
WST, Weighted Slab Technique.
ZAMS, Zero Age Main Sequence.

Outline

> The real voyage of discovery
> consists not in seeking new lands
> but seeing with new eyes
>
> MARCEL PROUST

Since ancient times, from the beginning of humankind, human beings have shown a great curiosity and attraction for what they saw when looking up. For one reason or another, the quest for explanations of mystical nature (maybe justifications) for what surrounded human life as well as its destiny was searched outside the Earth. This mystical interest encouraged the observation of the night sky which, in time, together with other social and philosophical changes, lead to a rational interpretation of what they observed and, hence the formulation of the first cosmogonical models and then cosmological models.

Precisely, the legacy of these first sky observers, has been the curiosity for the extraterrestial space in search of answers to many different questions. Some of these questions formulated by several scientists, were the seeds for a new discipline sowed in the field of physics science: *Cosmic Ray Physics*.

Since the beginning of XX century, when *Cosmic Ray Physics* was born, this discipline has walk a long way along which some relevant discoveries have been made, such as the discovery of positrons, pions and muons among other particles. Actually, the most powerful accelerators in nature are not built by human beings on Earth, on the contrary, one has to find them in astrophysical objects such as stars, pulsars, quasars, etc..., so these objects are the best candidates if one wants to seek evidences for the existence of some exotic new particles which are predicted in different theories (grand unified theories, string theories, quantum gravity theories, etc...). Nowadays, *Cosmic Ray Physics* consist on a discipline with a great tradition allowing to gather several different topics of astrophysics and physics such as nuclear physics, cosmology and elementary particle physics. As a result *Cosmic Ray Physics* has become a very attractive subject which offers an opportunity to work on several topics such as the nucleosynthesis of cosmic rays (studying the astrophysical sites and conditions in which the nucleosynthesis processes can occur, as well as their caracterisation as a nuclear process), the injection process, the acceleration mechanisms, the propagation process and the detection of cosmic rays near the Earth.

During the 80's, a set of experiences on board of satellites were planned and carried out with the aim of studying the hadronic component of cosmic rays, specifically ultra heavy ions with charge higher than Iron. The present work is, therefore, linked to one of such experiences; the UHCRE (*Ultra Heavy Cosmic Ray Experiment*). Several stacks of sheets of solid state nuclear track detectors used in the UHCRE have been analysed and measured by our group, recognizing a total of 205 tracks as originated by ultra heavy cosmic ray ions. The identification of cosmic ray ions recorded in UHCRE has been the first motivation of this work, so the first half of the present thesis deals with this problem.

The abundance of ultra heavy cosmic rays with $Z \gtrsim 65$ given in this work represents a statistically significant sample of such nuclei which is comparable to the total of data accumulated in all former experiments. This fact, has stimulated us to make the following question: Which is the source composition that, after propagation through the Galaxy, better reproduces our UHCRE measured abundances? To answer this question, it has been necessary to take a propagation model and then solve the corresponding transport equations. This task constitutes the second half of this work.

Therefore, the present Ph. D. thesis is divided into two parts: Chapters 1 and 2 cover the identification problem of the ions recorded in the UHCRE and, on the other hand, chapters 3 and 4 deal with the propagation process of the abundances of such ions back to their sources using the *Leaky Box model*.

I have decided to write this thesis in four independent chapters, in which all chapters follow a scheme of a scientific article, so each chapter has its own introduction, results, conclusions and references, as can be seen in the table of contents. There are two reasons for what I have adopted this arrangement rather than a classical design: firstly, the fact that a chapter is independent of each other allows to attack the document at any chapter and proceed to its reading without worrying about having read the previous chapters (actually, this is obvious for the first chapter, as happens with all thesis); and in second place, the article structure of each chapter makes its comprehension easier, as a significant amount of the scientific literature consists on papers written according this scheme. So, I have found worthwhile to use this organisation in each chapter in order to help for a quick localisation of what one is interested for.

The arrangement of the thesis goes as follows:

In chapter one, an identification method, known as *Reduced Etch Rate Fractional Gradient* (RERFG) is presented and a detailed study of its range of applicability is performed. The determination of the abundances of ultra heavy cosmic ray with $Z \gtrsim 65$ seen by the UHCRE is carried out using this method, because its conditions of applicability are fulfilled by the UHCRE experiment.

In the second chapter, an alternative track formation model based on a modification of the *Restricted Energy Loss* model is taken into consideration by introducing in the energy loss expression the close collisions corrections appearing in the corrected Bethe-Bloch formula, modulated by a new parameter. Then, the model is included in the charge assignation procedure, and a study taking the UHCRE measurements allows to establish relationships between the parameters involved in the identification process. Finally, an estimation of these parameters is made using experimental data from accelerator.

In chapter three, the transport equation for the *Leaky Box Model* (LBM) is deduced from the general transfer equation which describes the variation of the chemical composition of cosmic rays during their travel through the Galaxy. Detailed expressions of all parameters that take part in the propagation equations are provided, and the source abundances inferred from the UHCRE results are estimated solving the transport equations, corresponding to all elements with charge $65 < Z < 92$, with a numerical method that has to be understood as a first approximation to the problem.

In the last chapter, the *Leaky Box Model* transport equations are numerically solved using the *Weighted Slab Technique*, obtaining an excellent agreement with analytical solutions. A study of the response of the LBM is presented when different expressions of the required propagation parameters, such as the spallation cross sections, the path length distribution functions or the type of source composition. By optimizing the χ^2 statistical parameter between experimental and calculated abundances, it has been possible to determine which combination of all available expressions of the propagation parameters better reproduces the experimental abunadances of UHCRE.

Finally, the main conclusions of the present work are enumerated and can be found at the end of this document.

1. Identification and measurement of abundances of Ultra Heavy Cosmic Ray Nuclei detected by the UHCRE experiment

> Physical concepts are free creations of the human mind,
> and are not, however it may seem,
> uniquely determined by the outside world.
>
> ALBERT EINSTEIN

1.1. Introduction

1.1.1. History of Cosmic Ray research

The most relevant discoveries and experiments, which have been realized through the history in cosmic ray research are summerised in figure 1.1. A more detailed explanation of such events is developed in this section.

The precedents

The story begins about 1900 when the ionisation and electrical conduction of gases was under study. Many important new discoveries had been made in the preceding years. In 1897 Thomson succeeded in showing that cathodic rays had an electronic nature. Natural

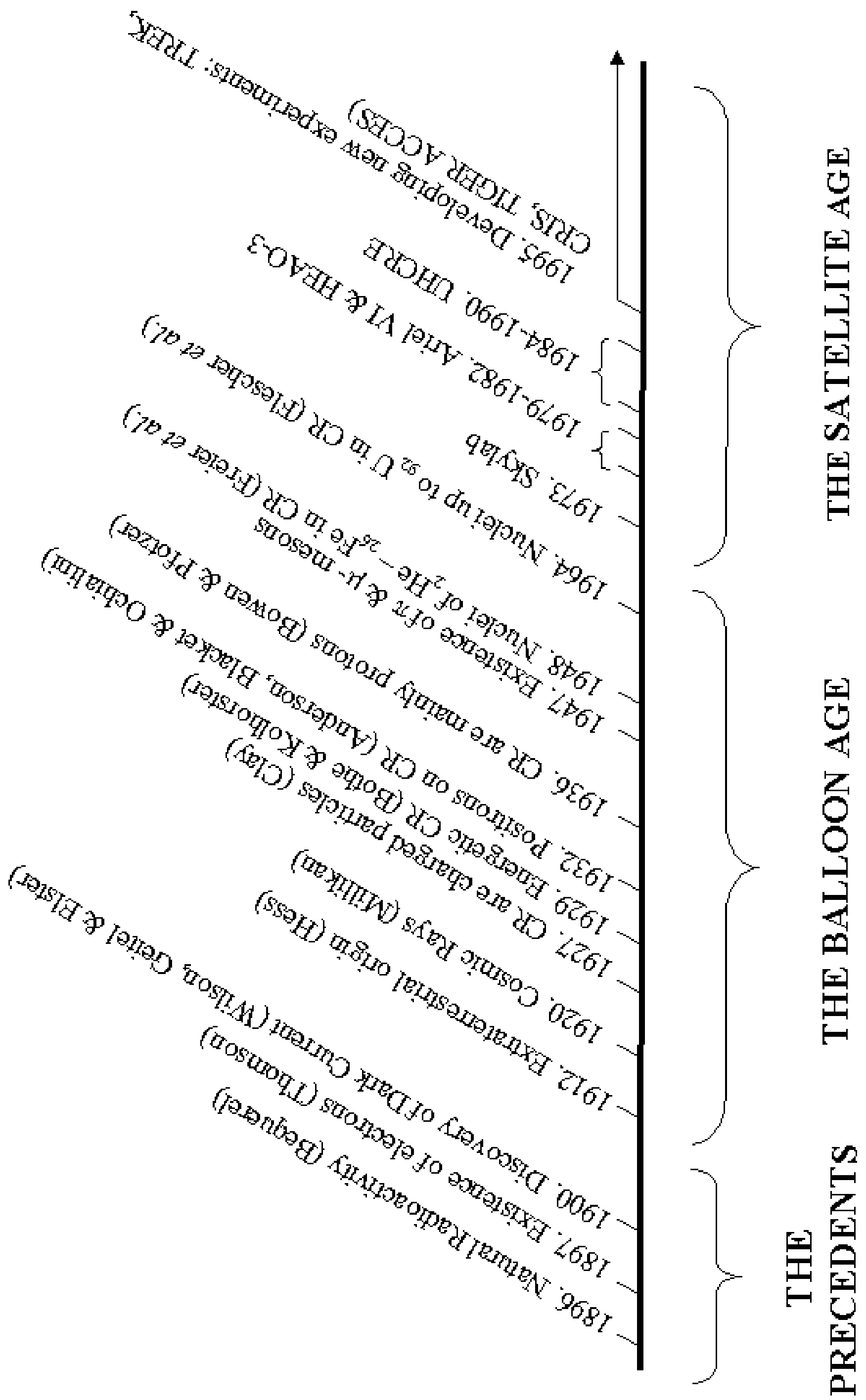

Figure 1.1. Main events in cosmic ray research chonologically displayed. Each tick points to the year, the event and its protagonists.

radioactivity had been discovered by Bequerel in 1896 and it was soon shown that the radiation consisted of three types of particles, the α, β and γ radiation.

The way in which the amount of ionisation was measured was by noting the rate at which a gold leaf electroscope lost its charge. Simultaneously, in 1900, Wilson, Geitel and Elster found that electroscopes kept discharging even if they were situated in the dark well away from the sources of natural radioactivity. This unknown radiation was called *dark current*.

At this point the question was, which is the origin of such *dark current*? It was thought that the bulk of the ionisation observed arose from γ rays emitted by radioactive elements present in the Earth. In 1910, Wulf (who was the responsible of the best electrometers used) found out that the ionisation fell from 6.0 ions/s·cm^3 to 3.5 ions/s·cm^3 as he ascended the Eiffel Tower (330 m). Consequently, this result seemed to confirm the previous hypothesis but γ rays should be halved in 80m of air.

The balloon age

The real breakthrough came in 1912 and 1913 when first V. Hess in Vienna and then Kolhörster in Berlin made manned balloon ascents in open balloons, carrying their detection instruments to altitudes of 5 km and eventually 9 km. They discovered that the intensity of the radiation effect on their detectors drastically increased with altitude so conclude that the radiation was originated at, or outside of the upper atmosphere. Since the radiation persisted day and night, it was also concluded that the sun was not the direct source.

In the twenties, A. Millikan, who coined the name "**COSMIC RAYS**" for the mysterious radiation, showed that the atmosphere behaved as a mass of absorbing material, and consequently was not the producer of primary cosmic rays. He observed that the radiation was absorbed in water to the same degree as in an equivalent weight of air. He also confirmed, with improved measurements, the dependence of ionisation with altitude as can be seen in figure 1.2.

The hypothesis for the so-called cosmic rays was that they consisted on γ rays with a bit more penetrating power than that observed in natural radioactivity and the extra ionisation was caused by elastic scattering with atomic electrons. Nevertheless, Clay, in 1927, found that the intensity of cosmic rays is smaller near the Earth's equator than towards the polar regions. This was interpreted as a deflection due to the geomagnetic field, so, in consequence, it was concluded that radiation consisted of charged particles.

By the late part of this decade, new research techniques were being used. For instance, the Geiger-Müller detector, which enabled individual cosmic rays to be detected, was invented in 1929. Skobeltzya used cloud chambers to study cosmic rays. On the other hand, Bothe & Kolhörster used two Geiger-Müller counters, one above the other, and found that simultaneous discharges of both detectors occurred very frequently. Using multiple counters and absorbers they conclude that charged particles of cosmic rays were very fast

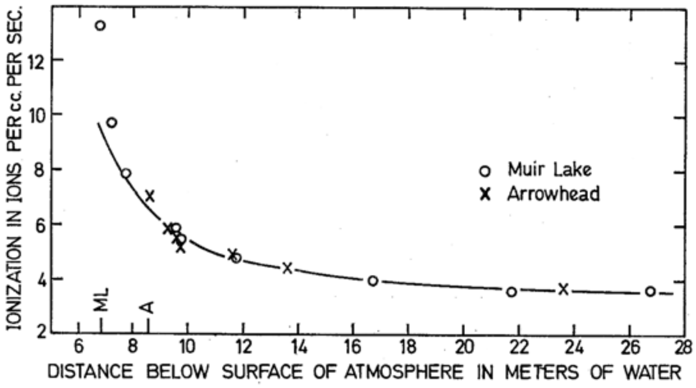

Figure 1.2. The observations of Millikan and Cameron with electrometers. ML & A mark the lake surfaces [Hil72].

or energetic.

In the 1930's, large electromagnets were being used in conjunction with cloud chambers and Geiger-Müller counters. From the curvature of the tracks it was immediately apparent that many of the particles had energies of $\sim 10^9 - 10^{10}$ eV and many were so energetic that no appreciable deflection took place. Anderson in 1932, and Blackett & Occhialini in 1933 showed that in the cosmic radiation existed positively charged particles very similar to electrons and this proved to be the discovery of positrons. Simultaneously, an east-west asymmetry in the intensity of cosmic rays was observed at various altitudes by Johson and Alvarez & Compton. This fact led to the conclusion that practically all primary cosmic rays are positively charged. As this asymmetry increased with altitude, it seemed to suggest that these particles could be protons. That hypothesis was supported by measurements supplied by Bowen and Pfotzer in 1936, who found out that charged particles of cosmic rays are heavier than the electron. Schramm in 1941 confirmed, using counters telescopes with absorbers, that particles impinging upon the atmosphere (called *primary radiation* or *primary cosmic rays*) consist mainly in protons.

Evidence for particles closely resembling the mesons predicted by Yukawa were found in the late 1930's and measurements of the amount of ionisation led to estimates of their mass about 200 times the electron mass.

In the forties, nuclear emulsions, scintillator counters, sophisticated electronics and high altitude balloons were incorporated into cosmic ray research. A big advantage of nuclear emulsions is that being much denser than the gas in a cloud chamber, there is a much higher probability of observing interactions in the emulsions. In 1947 π- mesons and μ-mesons were discovered using these nuclear emulsions.

The late 1940s and early 1950s were a particularly exciting epoch in cosmic ray physics since cosmic rays provided a readily available source of very high energy particles so that many new types of particles were discovered. Among them: $\kappa^+, \kappa^-, \kappa^0, \Lambda, \Sigma^+, \Xi^-$. In the 1950s, accelerators took over the detailed investigation of elementary particles under more carefully controlled conditions.

Also in the late of the decade of 40s, Freier and collaborators made several high altitude balloon experiments using nuclear emulsions. Their results showed that protons of primary cosmic radiation were accompanied by nuclei of elements from Helium to Iron ($z \leqslant 28$). This discovery opened the possibility of studying, at first hand, a sample of matter from elsewhere in our Galaxy.

Flescher *et al.* analysed tracks of nuclei in meteorite crystals which were exposed to primary cosmic radiation for long periods of time, discovering that these tracks were originated from arriving nuclei heavier than iron ($z > 28$), the so-called *Ultra Heavy Cosmic Rays* (UHCR).

In order to work with statistically significant samples of ultra heavy nuclei of the primary cosmic radiation, nuclear track plastic detectors and nuclear emulsions of high area had to be developed due to the low arrival flux of such particles which its composition were studied, since then, employing detectors characterised by their low area and short time of exposition. Fowler *et al.* set up in balloons this kind of passive detectors and made some high altitude ascents, obtaining nuclear tracks originated by UHCR nuclei with atomic number up to Uranium ($Z = 92$). In consequence, charge spectrum was extended from Iron through the rest of the periodic table of elements up to Uranium.

The satellite age

The decade of the 1970s saw the design and development of several experiments which were mounted on board of satellites and had the aim of studying the composition and energy spectra of the arriving UH nuclei which belong to the primary cosmic radiation with an improved quality of the data obtained.

The first of such experiments was the Skylab [Pri75], [Shi78] which was launched for the first time in 1973 and the following year for second time. The aim of the Skylab experiment was to measure the charge and energy spectra of UHCR with $Z \geqslant 60$. For such purpose, Lexan track recording plastic sheets displayed in stacks were used. The Skylab spacecraft was exposed for 253 days in a circular orbit at an average altitude of 430 km. A total of 104 tracks originated by UHCR nuclei with $Z \geqslant 65$ were observed. The analysis of the data obtained showed a median charge resolution of 3.1%. Charge spectra obtained in the Skylab experiment is illustrated in figure 1.3.

In 1979, two new experiments were launched into the Earth orbit, one of them was the Bristol cosmic ray detector on the Ariel VI satellite, and the other one was the High Energy Astronomy Observatory (HEAO-3). In both experiments, electronic detectors with low value of the area-solid-angle factor but with a good charge resolution (~ 0.3 to 0.5 charge units) were employed.

The Ariel VI satellite [Fow85], [Fow87] was launched by NASA on 3rd June 1979

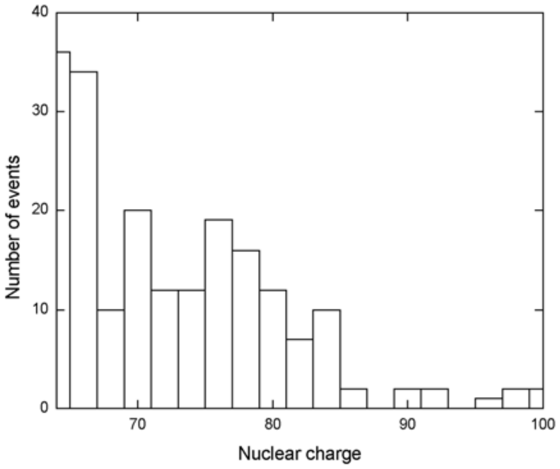

Figure 1.3. Final charge spectrum for Skylab detector. Data are grouped into bins of two charges.

into near circular 625 km orbit. The last data from Ariel VI were received in February 1982, but spacecraft problems restricted data collection to only 427 of the days in orbit, corresponding to 352 complete days at 100% efficiency. The detector was designed to measure the composition of UHCR with $Z > 34$ and consisted basically on a spherical aluminium vessel containing a gas scintillation mixture and a thin spherical shell viewed by photomultipliers. A plastic scintillator was also used as an anticoincidence detector in order to characterize particle tracks through the detector. Figure 1.4 illustrates the charge spectra for the highest charges ($Z \geqslant 70$) plotted from results of the Ariel VI experiment.

The detector designed for the Heavy Nuclei Experiment (HNE) flown on the HEAO-3 spacecraft [Bin82], [Sto87], [Bin89] consisted of ionisation chambers, multi-wire ionisation hodoscopes and a Cerenkov detector. The threshold of the detector together with the orbit characteristics ensured that at least 80% of the observed nuclei with $Z \geqslant 70$ had energies over 1 GeV/nucleon. HEAO-3 was launched on 20th September 1979 into a 500 km orbit and operated for 580 days until 30th May 1981. The charge resolution achieved with this instrument was 0,6 e (e is the electron charge taken as the charge unit). A total of 62 nuclei were detected in the charge region $70 \leqslant Z \leqslant 86$ [Fix83], [Bin85], which is enlarged up to 300 nuclei when the charge region is extended to $50 \leqslant Z \leqslant 86$. Figure 1.5 shows the charge spectrum obtained from measurements of the HEAO-3 experiment.

The last experiment was the *Ultra Heavy Cosmic Ray Experiment* (UHCRE) which was deployed into Earth orbit in 1984 aboard *Long Duration Exposure Facility* (LDEF). Due to the loss of the space shuttle Challenger, the LDEF remained in Earth orbit until early 1990 and was retrieved successfully by a second shuttle mission after approximately 69

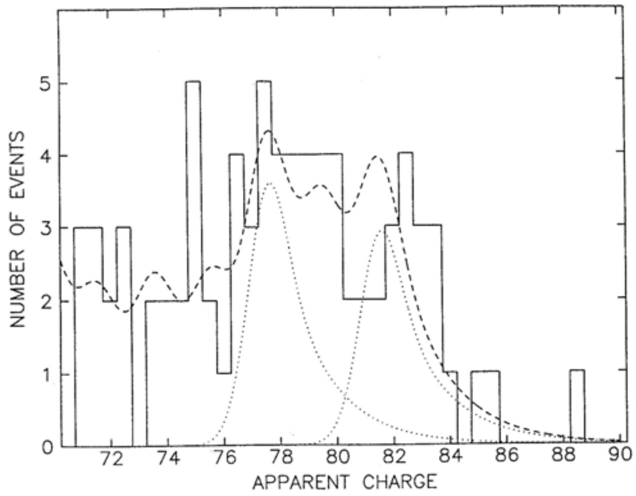

Figure 1.4. Distribution of accepted data for determination of $Z \geqslant 70$ abundances. Dotted inserts show the two abundance peaks for the Pt ($Z = 78$) and Pb ($Z = 82$) obtained deconvolving the observed data.

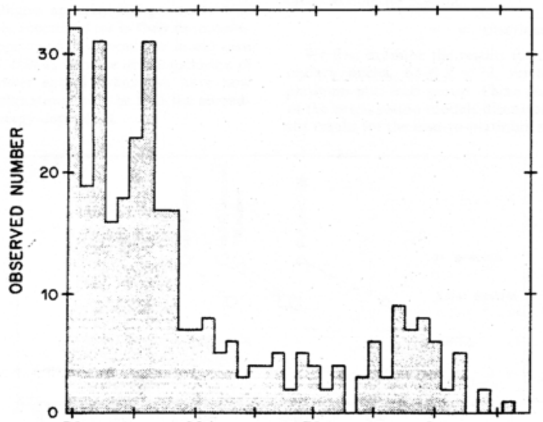

Figure 1.5. Observed charge spectrum from HEAO-3 measurements analysis.

months in space. The extended duration of the LDEF mission resulted in the collection of approximately 10 times the previous world sample of UH nuclei with $Z > 65$, in consequence the most statistically relevant sample of such ions has been obtained in the UHCRE.

At present the next generation of experiments aboard satellites are being designed in order to study the highest charge region with high resolution measurements. The purpose of *TREK* experiment is to measure the isotopic and the elemental composition of the galactic cosmic rays [Wes95]. The *Cosmic Ray Isotope Spectrometer* (CRIS) instrument is aimed to measure the isotopic abundances of the galactic cosmic rays with charge comprised between 3 and 30 and energy per nucleon between 50 and 500 MeV/n [Ros97]. The *Trans-Iron Galactic Element Recorder* (TIGER) experiment has been designed to measure the elemental abundances of UH cosmic rays with charge $26 \leq Z \leq 92$ [Bin95], [Spo00]. Cherenkov counters used in TIGER experiment will also be included in the UH module of the *Advanced Cosmic-ray Composition Experiment for the Space Station* (ACCES) [Bin97] which has as a main goal to extend its detection range to other particles among UH cosmic ray nuclei [Isb97].

1.1.2. Properties of Primary Cosmic Radiation

Composition and energy spectrum are the two main features of the arriving cosmic rays at the top of the atmosphere, the so-called Primary Cosmic Rays (PCR) which are free from any secondary cosmic rays produced in our own atmosphere. In this section those aspects that are relevant for the UHCRE experiment are introduced.

Energy spectrum of cosmic rays

The energy spectrum of PCR extends over 14 orders of magnitude and can be divided into four characteristic regions:

i) The first region corresponds to energies below $\sim 1 - 2$ GeV/n. Solar modulation processes, which are due to the effect of solar wind on particles travelling near the Sun, are important at these energies. The 11 year solar circle during which the number of sunspots and also the general solar activity oscillates, allows to give evidence for solar modulation. Figure 1.6 shows clearly the correlation (rather anticorrelation) between the intensity of neutrons measured by the Mount Washington neutron monitor and the relative sunspot number, which accounts for the solar activity [She85].

Furthermore, the shape of the spectrum of Hydrogen and Helium nuclei in PCR, as a function of phase of the solar cycle is illustrated in figure 1.7. In each set of spectra, the top curve shows the measurements at the time of the minimum sunspot number and the bottom curve at sunspot maximum [Web74].

ii) The second energy region extends from $\sim 1-2$ GeV/n up to $\sim 10^6$ GeV/n. The spectrum of Hydrogen, which is the most abundant nuclei of PCR, at these energies (see figure 1.8) can be described quite well by a differential power law in energy of the form

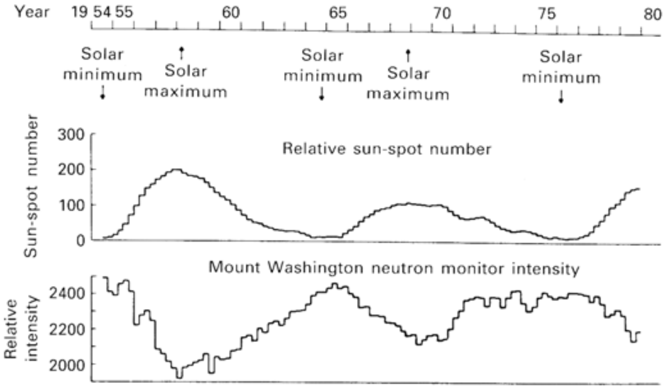

Figure 1.6. The correlation between the relative sun-spot number and the intensity of measured neutrons.

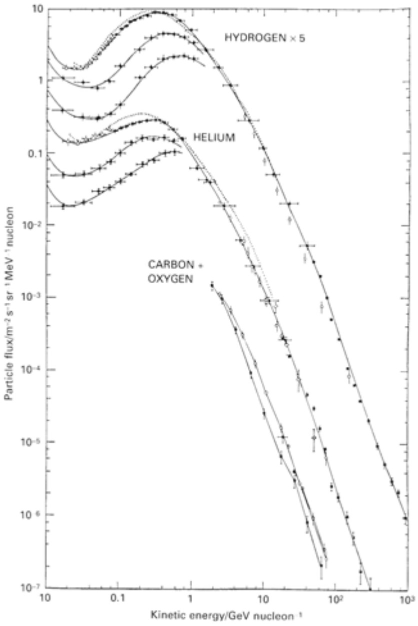

Figure 1.7. The differencial energy spectra of Hydrogen and Helium nuclei in the cosmic rays as a function of phase of the Solar cycle. In each set of spectra, the top and the bottom curve correspond to sunspot minimum and maximum respectively.

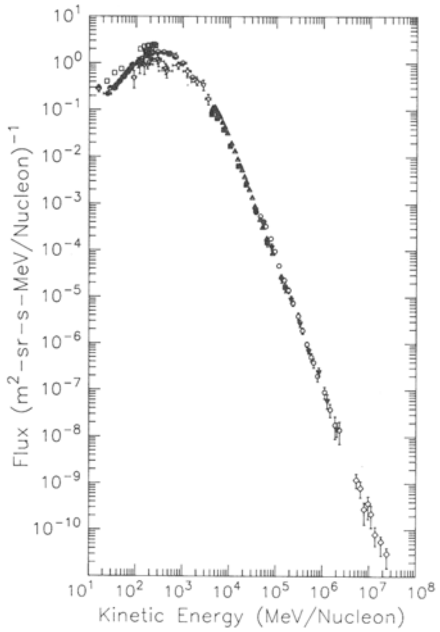

Figure 1.8. The differential energy spectrum for cosmic ray protons following a differential power law.

[Wef88]:

$$N(E)dE = k \cdot E^{-2.7}dE$$

The spectrum of other heavier elements shows the same behaviour than that of hydrogen, as can be seen schematically in figure 1.9 [Sil90].

*iii)*The next energy region corresponds to energies between 10^6 GeV/n and 10^{10} GeV/n. In order to study the energy spectrum in this region, the Earth's atmosphere is utilized as a target and products produced in the resulting extensive air shower are measured. When a very high energy single cosmic ray penetrates the top of the atmosphere a shower of secondary cosmic rays is developed, such events are called *Extensive Air Showers* (EAS). In figure 1.10 [Boo97] the modified flux of PCR is plotted in terms of the total energy in PeV units, it is clearly inferred from this figure a break in the power law spectrum around ~ 4 PeV ($4 \cdot 10^6$ GeV) which is known as the "knee".

The origin of the knee remains as an open question, known as the so-called "knee problem", so that many different models have been proposed which can be divided into two distinct classes [Erl01]: *astrophysical* and *interaction* models. Interaction models assume that the primary energy spectrum has no sharp change and the observed steeping of EAS size spectra is due to the sudden change of the nature of the interactions between the high energy particles of PCR and the atmosphere. Astrophysical models attribute the change

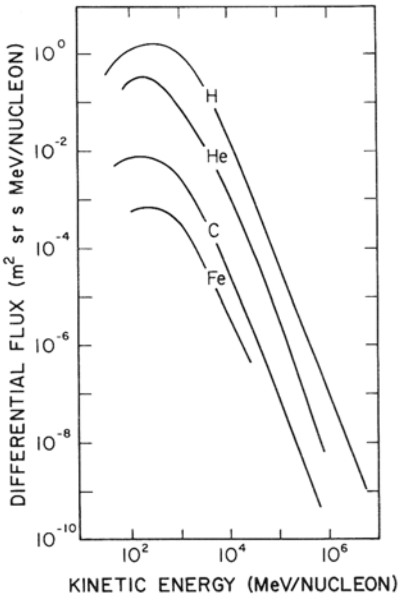

Figure 1.9. The energy spectrum of several elements (H, He, C and Fe) measured at the Earth.

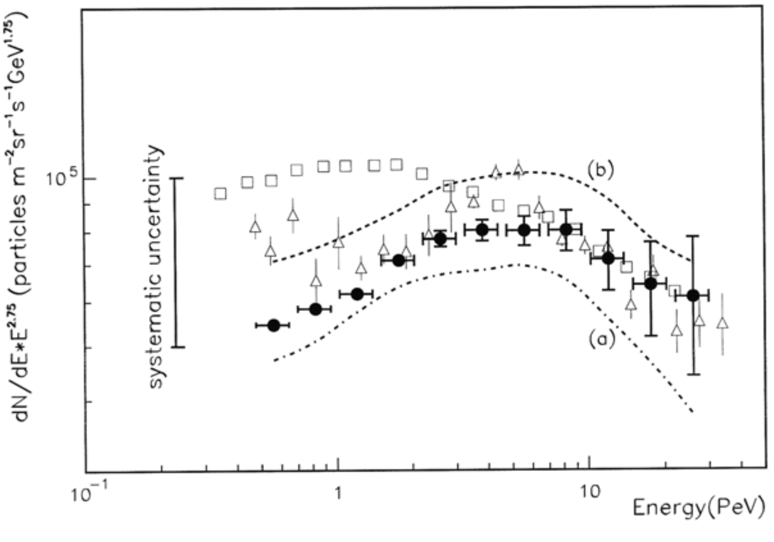

Figure 1.10. The absolute fluxes of cosmic rays obtained from EAS measurements. Note that the fluxes are multiplied by a factor of $E^{2.75}$. Each PCR spectrum curve shows a maximum corresponding to the knee where a sudden steeping is ocurred.

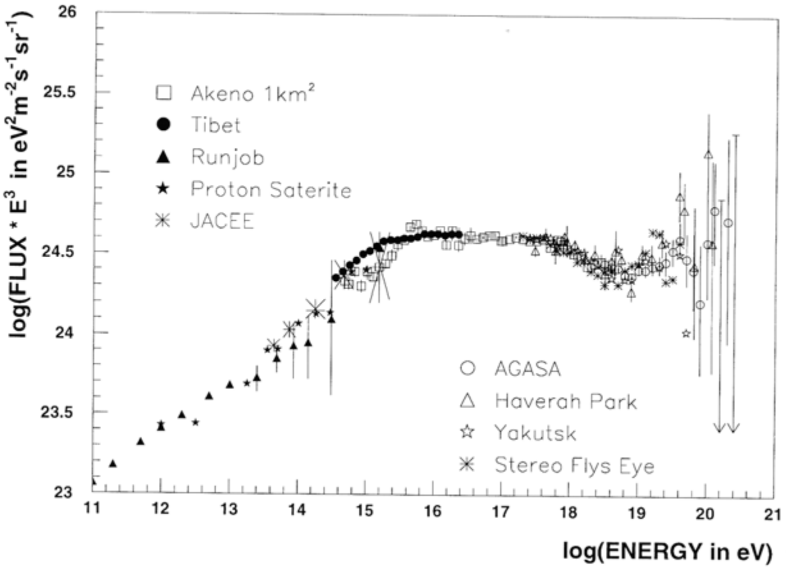

Figure 1.11. The CR all-particles spectrum observed by different experiments above $10^{11}eV$. The differential flux in units of events per area, time, energy, and solid angle has been multiplied with E^3 to project out the steeply falling behaviour.

in the energy spectrum of the observed EAS to the change in the energy spectrum of PCR while travelling from source to Earth's atmosphere. As this kind of models are the more developed, they might be also subdivided into *source* models, which assume that the breaking in the spectrum takes place in the source region or is caused by the acceleration mechanisms, and the *propagation* models considering that the propagation process from source to the observer is the responsible of such breaking.

iv) The highest energy region corresponds to energies above 10^{10} GeV/n. Cosmic Ray spectrum at these ultra high energies showed in figure 1.11 is well approximated by broken power laws $\propto E^{-\gamma}$. Cosmic rays with this energy are usually attributed to an extragalactic origin. Nevertheless the main problem is to find out the astrophysical scenarios leading to cosmic ray acceleration up to such ultra high energies. Several acceleration processes have been proposed in literature [Ber97], [Ost00], [Sig01].

Composition of Cosmic Rays

Primary Cosmic Rays include all kind of particles from outer space that reach the top of the atmosphere, which can be classified into four groups [Wef88]:

i) *Electrically charged particles*: Both positive and negative. This include electrons, positrons and the nuclei of the elements of the periodic table from Hydrogen, which is the most abundant up to the actinides group (with $Z \sim 92$). Figure 1.12 shows the

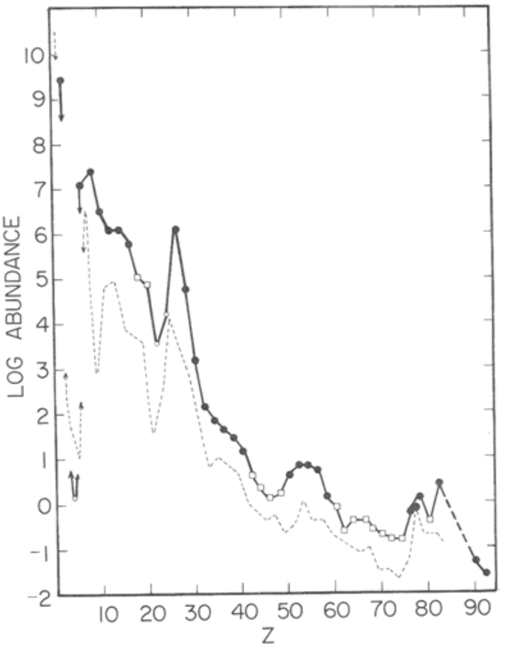

Figure 1.12. Relative abundances of the elements. Solid line connects even-Z elements and dashed line connects odd-Z elements.

relative abundance of these nuclei belonging to the PCR [Isr83], solid line connects even-Z elements and dashed line connects odd-Z elements showing, clearly, the so-called *odd-even effect* which is a consequence of the different nuclear stability for even-Z nuclei and odd-Z nuclei. The other main feature of PCR nuclei shown in figure 1.12 is the relative abundance between Iron and Hydrogen with a value $\simeq 10^{-6}$, and between Uranium and Iron with a value $\simeq 10^{-6}$ (so that it arrives 1 nuclei of Uranium per one billion of Hydrogen nuclei). Thus, the low abundance of the heaviest nuclei in PCR has to be taken into account in order to collect a statistically significative sample of such nuclei.

ii) *Electrically neutral particles.* This include neutrons, neutrinos, neutral mesons and hyperon, and, possibly yet undetected particles such as the magnetic monopole which is predicted by Grand Unified Theories, or even the photino predicted by Supersymetric Theories.

iii) *Electromagnetic quanta.* Here, only photons with any energy of the electromagnetic spectrum are included. These photons are the basis of astronomical research. At ground level, only photons with energy smaller than the optical and ultraviolet ones can be observed, so, high energy photons (mainly X-rays and γ-rays) have to be studied near the top of the atmosphere by means of balloons, rockets or artificial satellites.

iv) *Dust particles.* There is wide variety of materials constituents of the dust which is generally assumed to be well coupled to the cosmic gas. Some of these are volatiles in the form of frozen ices, the rest are relatively non-volatile or refractory. However even the refractories have varying degrees of volatility. The major refractory components which have been observed may be characterized as silicates and organics [Gre91]. Cosmic dust has been studied on high flying aircraft, balloons and space missions.

1.2. The UHCRE experiment

The Ultra Heavy Cosmic Ray Experiment (UHCRE) has been the largest array of cosmic ray particle detectors ever flown in space [Tho87], [Tho91], [Tho92], [Osu88], [Osu92]. It comprised 192 Solid State Nuclear Track Detectors (SSNTD) stacks, housed in 48 pressurized vessels (at 1 atm. of dry air) mounted in 16 experimental trays on board the NASA Long Duration Exposure Facility (LDEF), this experimental set up is illustrated in figure 1.13 and figure 1.14 shows the final appearence of one UHCRE tray once mounted. The UHCRE was designed by the *Cosmic Ray Group* of the *Dublin Institute for Advanced Studies* in collaboration with the ESTEC of the *European Space Agency* (ESA). Figure 1.15 consist on a picture of the LDEF satellite, containing all the experiments on board on 86 experimental trays, before to be launched. The LDEF was launched into Earth orbit, at height of approximately 450 km and an inclination of 28.5° with respect to the equatorial plane, in April 1984 by the NASA Space Shuttle Challenger and retrieved in January 1990 at height of approximately 325 km by the Space Shuttle Columbia. In figure 1.16 the LDEF satellite is in a stabilized terrestrial orbit, the trays corresponding to the UHCRE can also be distinguished Each UHCRE stack was (20×26) cm^2 in size and contained mainly Lexan polycarbonate plates (~ 250 μm thick each) interleaved with several lead plates (~ 500 μm thick) used as absorbers. Nevertheless, some stacks did not contain lead plates and included some CR-39 (pure, DOP and DIOP) plates. The Lexan equivalent thickness of all UHCRE was comprised between ~ 4 g/cm^2 and ~ 6 g/cm^2 with an average value of 4.7 g/cm^2. The thermal design of the UHCRE was aimed at maintaining the temperature of the detectors below 30°C and ensuring as narrow a band as possible between maximum and minimum values. This was successfully achieved by the use of silvered Teflon thermal blankets and by thermally decoupling the detector vessels from the LDEF frame. Temperatures were measured at selected locations on the LDEF structure during the first 490 days of history of the UHCRE stacks. The results of this analysis show that the detector stacks were maintained below 0°C throughout the mission. The maximum detector stack thermal gradient was 0.15°C per stack.

The geomagnetic cutoff of the LDEF orbit ensured that no ion with energy below $\sim$ 3 GeV/n was present in this orbit. On the other hand, the Lexan registration threshold was such that only ions with $Z > 65$ of the energies involved in the LDEF orbit were recorded. Consequently, the much more abundant iron, C-N-O and proton cosmic ray components could not be registered by the UHCRE detectors.

The main purpose of the UHCRE was to determine the elemental abundances

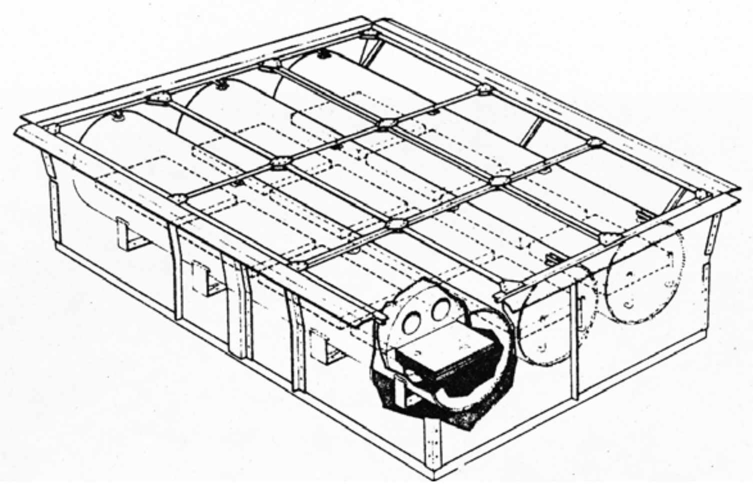

Figure 1.13. Experimental set up of the presurized cilinders of each of the 16 trays of the UHCRE. Every cilinder contains 4 stacks of SSNTD's.

Figure 1.14. Final aspect of a tray of the UHCRE experince once mounted and before to be boarded on LDEF.

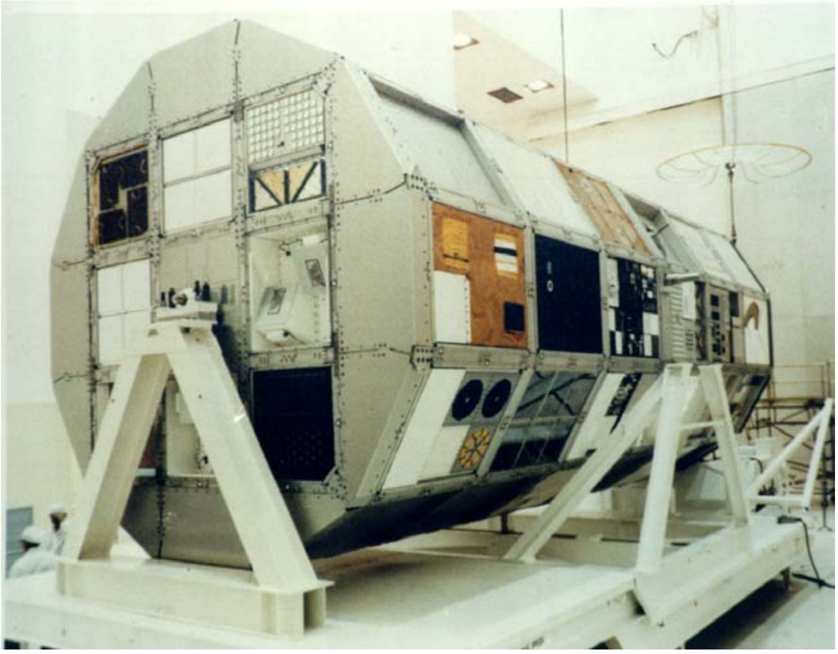

Figure 1.15. Picture of the LDEF satellite with the 76 trays containig all experimets, before to be launched in terrestrial orbit by means of the Challenger spacial shuttle.

Figure 1.16. LDEF satellite once deployed in space and stabilized on a terrestrial orbit. Several UHCRE trays can also be seen.

of ions with $Z > 65$ present in cosmic rays. Over 2500 UH ions with charge over 65 have been recorded in the UHCRE after its approximate six-year exposure in space. This number represented about 10 times the total number of such ions ever recorded in all former experiments, mainly Ariel-VI and HEAO-3 and would include the first statistically significant sample of actinides [Tho93, RM96],[Osu95a, RM96]. A total of 205 tracks have been located, measured, and positively identified as originating from cosmic ray ions with $Z > 65$ in the 10 detector stacks analyzed by our group in *Universitat Autònoma de Barcelona*. The number of events recorded in this sample alone is similar to the world UH sample collected in all former experiments [Dom95].

1.3. Measurement and analysis of the UHCRE.

When an incident ion penetrates a stack of plastic detector plates, it generates a latent track due to the damage done to the structure of the plastic material along its trajectory. Latent tracks in the plastic detector of the UHCRE were made visible under an ordinary microscope chemically etching the plates.

The knowledge of the processes involved in latent track registration and its visualization through etching is essential in order to perform a correct identification of the registered particles and to establish the uncertainty associated to this procedure. The main purpose of the present work is to analyse various methods of charge assignment for particles recorded in Solid State Nuclear Track Detectors (SSNTD). The results of this analysis may be used to ascertain the possibility of separating the peaks due to r and s processes in UH cosmic ray registration experiments where SSNTDs were used, such as the UHCRE.

1.3.1. Identification of charged particles

Stopping power and track formation

The registration of ions using SSNTDs is based on its passage through several stacked plates of dielectric track detectors. Several metal plates (lead, iron, aluminium,...) may be interleaved in the stack in order to increase the stopping power. The specific energy loss $-\frac{dE}{dx}$ (energy loss per unit of path length) of a charged particle in a given absorber due to electronic collisions is described by the Bethe-Bloch equation [Fan63], [Ahl82] and depends, mainly, of the detector composition and density and of the incident particle charge and energy. According to the *Restricted Energy Loss* (REL) track formation model [Ben68], [Ben69], the latent track formation is due only to the energy deposited by the distant collisions of the incident particle with the absorber electrons. Distant collisions are defined as those originating recoil electrons with low energy (ω), smaller than a fixed value (ω_0) that depends on the absorber, that deposit their energy in the neighbourhood of the path followed by the incident particle. The value of the energy ω_0 that separates distant from close collisions is such that for close collisions the absorber atomic electrons may be considered as free particles, whereas for distant collisions the incident particle may be treated as a point charge. In practice, ω_0 is obtained from the best fit to experimental data.

The Bethe-Bloch formula used in our calculations, which is known as the *uncorrected* Bethe-Bloch formula, can be written as follows:

$$-\left(\frac{dE}{d\xi}\right) \equiv \frac{4\pi N_A e^4}{m_e c^2}\frac{Z_1^2}{\beta^2}\frac{Z_2}{A}\left\{\ln\left(\frac{2m_e c^2}{I_0}\frac{\beta^2}{1-\beta^2}\right) - \beta^2 + \psi(1) - \mathrm{Re}\,\psi(1+i\nu)\right\} \tag{1.1}$$

where $d\xi = \rho dx$, being ρ the density of the absorber and x the path length of teh incident ion, Z_1 is the charge of the incident particle, Z_2 is the charge of teh absorber atoms, $\beta = v/c$ is the velocity of the incident particle (v) in units of the velocity of light ($c = 2.99792458 \times 10^8\,\mathrm{m\,s^{-1}}$), $m_e c^2$ is the electron rest mass ($0.51099906\,\mathrm{MeV}$), I_0 is the mean ionisation potential of the absorber. $\psi(1) - \mathrm{Re}\,\psi(1+i\nu)$ is the quantic Bloch correction.

According to the model described, the energy transferred from the incident charged particle to the absorber electrons is split into two parts

$$-\frac{dE}{d\xi} = -\left(\frac{dE}{d\xi}\right)_{\omega<\omega_0} - \left(\frac{dE}{d\xi}\right)_{\omega>\omega_0} \tag{1.2}$$

where the first term corresponds to distant collisions and contributes to latent track formation, and the second one is the close collisions term, not contributing to track formation. The Bethe-Bloch equation 1.1 may be written in a form that the terms of equation 1.2 are easily identified as

$$-\left(\frac{dE}{d\xi}\right)_{\omega<\omega_0} \equiv REL_{\omega_0} = \frac{4\pi N_A e^4}{m_e c^2}\frac{Z_1^2}{\beta^2}\frac{Z_2}{A}\left\{\frac{1}{2}\ln\left(\frac{2m_e c^2}{I_0^2}\frac{\beta^2}{1-\beta^2}\omega_0\right) - \frac{\beta^2}{2}\right\} \tag{1.3}$$

Description of the ion identification procedures

The latent track, which consists on a sub-microscopic damage of the detector chemical structure in a very small region around the incident particle path, starts at the entrance point of the ion in the stack and ends either at the point where the ion stops inside the stack or at the point where it escapes from the stack. This sub-microscopic damage is visible only under very powerful electron microscopes. A chemical etching of the detector is performed in order to make the latent track visible under an ordinary optical microscope. The etching process of the detector plates leads to the formation of two typically cone-shaped etch pits in each plate traversed by the incident particle, one on each side of the plate (entrance cone and exit cone). The geometry of these cones is due to the combination of two etching processes: the chemical dissolution along the particle track at a linear rate v_t, and the general attack on the etched surface and on the interior surface of the etched track at a rate v_b [Fle75], [Dur87]. The position of these cones in the plates allows to reconstruct the path of each incident ion through the stack. A quantity x_i may be defined as the distance from the entrance point of a given ion in the stack to the center of the i-th cone of its track. Geometric measurements of the cones allow to determine the track etch rate $v_{t,i}$ and bulk etch rate $v_{b,i}$ for each of them, and therefore to calculate the reduced etch rate $S_i = \frac{v_{t,i}}{v_{b,i}}$. This quantity S_i accounts of the detector response at a given point and is the magnitude that gives the value of signal strength. Hence, a given track originated by an incident ion is characterised by set of (x_i, S_i) points.

The information contained in this set of points can be used to identify every recorded particle and to calculate the associated charge uncertainty, assuming a relationship between the reduced etch rate S and REL_{ω_0}. Several expressions for this relationship has been developed in former works, but it has been found that the most appropiate function which fits S with REL_{ω_0} has a potential form [Fle75], [Seq76], [Fer81], [Luc82] and [Vid84] :

$$S = g\left(REL_{\omega_0}\right)^h \tag{1.4}$$

where g and h are constant parameters that must be obtained from calibration. This relationship is not necessarily valid over all possible energies of an incident ion of a given charge, but it is accomplished, at least, for any given small energy interval. In other words, the values obtained of g and h for a given charge may depend on the energy of the ion.

When a given particle penetrates a SSNTD's stack, three different behaviours are possible depending on the charge and energy of the incident particle and on the stack thickness. There is at least one identification method available for each of them:

i) Particles which come to rest in the stack. The particle energy and the stack thickness are such that all energy is transferred to the detector, so the particle comes to rest in it. In this case, the range of a particle R is calculated as the distance between its entry point in the stack and its stopping point. The residual range R_i at a given cone, defined as the distance from the centre of this cone to the ion stopping point, is calculated as $R_i = R - x_i$. The corresponding S_i value is obtained from geometric measurements. A method based in the S-R relationship can be used to identify such ions [Ben68], [Fle75] & [Dur87] from the experimental (S_i, R_i) set obtained for each recorded track.

ii) Particles which traverse the stack without loosing any significant amount of energy. The particle energy remains almost constant along its trajectory, therefore the reduced etch rate corresponding to all cones in a given track should be equal, and an a method based on the average S value $(\bar{S})$, which may be assigned to each track, can be applied to identify such ions [Dom95], [Dom96].

iii) Particles which traverse the stack, loosing a measurable amount of energy. This amount of energy lost is precisely the parameter which allows to identify the charge and energy of the incident particle. In this case, a method based on the reduced etch rate fractional gradient (RERFG), already proposed in [Fow77a], [Fow77b], can be employed for identification.

Consequently, a different identification method must be applied for each of the situations described above. As we are dealing only with non-stopping ions in the present work, only situations (*ii*) and (*iii*) are relevant.

If the particle registration conditions allow to assume that the reduced etch rate S remains constant along the particle path in the detector (situation (*ii*)), every complete single track originated by one ion in the detector stack can be characterised by an average S value ($\bar{S}$) instead of a set of (x_i, S_i) points, as the reduced etch rate does not display significant variations with the penetration distance x. If it is assumed that the restricted energy loss (REL_{ω_0}) is the physical magnitude responsible of latent track formation, REL_{ω_0} is proportional to $\frac{Z^2}{\beta^2}$, being Z the incident particle charge and β its velocity. Considering the relationship given in 1.4 and taking into account that β remains almost constant, $\bar{S}$ is strictly proportional to Z^{2h}, and therefore it is possible to obtain the charge distribution of the particles recorded from the distribution of average values, $\bar{S}$, of the reduced etch rate. The relationship between Z and $\bar{S}$ must be obtained from calibration. The main inconvenient of this method for charge assignation is that the charge scale is not linear with $\bar{S}$, so that it may not be straightforward to determine the charge uncertainty for a given uncertainty of $\bar{S}$, which, on the other hand, may also depend on the energy of the recorded particle. Moreover, a single measured parameter as the averaged reduced etch rate, $\bar{S}$, cannot provide information about two independent characteristics (charge and incidence energy) of the incident particle, so that it is necessary to make assumptions about one of them for determining the other one (*i.e.* it is necessary to have some knowledge of the energy of the incident ions in order to identify their charge).

Some of the drawbacks which arise from the above charge identification method may be overcome if one considers that there is a small gradient of specific energy loss along the incident particle path and, consequently, a small gradient of reduced etch rate (situation (*iii*)). The fractional gradient of reduced etch rate is defined as

$$G \equiv \frac{1}{S}\frac{dS}{dx} \tag{1.5}$$

According to this method [Fow77a], [Fow77b], each track is characterised by a single (S_{eff}, G_{eff}) couple, which is calculated from the measured set of points (x_i, S_i) using

$$G_{eff} = \left| \frac{\sum_{i=1}^{n} \left[\frac{2(S_{2n+1-i} - S_i) w_i}{(S_{2n+1-i} + S_i)\Delta x_i} \right]}{\sum_{i=1}^{n} w_i} \right| \tag{1.6}$$

where w_i is a weight function proportional to $(\Delta x_i)^2$, and

$$S_{eff} = \frac{n}{\sum_{i=1}^{n} \frac{S_i + S_{2n+1-i}}{2 S_i S_{2n+1-i}}} \tag{1.7}$$

In these expressions, it has been considered that each recorded ion passes across n plates of the SSNTD stack and, therefore, generates $2n$ cones (two cones per plate).

1.3.2. Application of the identification method based on the reduced etch rate fractional gradient (RERFG).

Charge assignment

In order to assign a charge to any given ion recorded in an experiment, each of the (S_{eff}, G_{eff}) points obtained using expressions 1.6 and 1.7 from the experimental geometric measurements in one given track should be compared to the $S_Z(G)$ curves, generated in the $G-S$ plane, for every different charge Z within the range of interest for the experiment performed. Obviously, determining which of the generated curves is closer to one (S_{eff}, G_{eff}) point allows to assign a value Z of charge to this point and, therefore, to the ion which has originated the track studied.

In practice, given expressions 1.3, 1.4 and 1.5, the $S_Z(G)$ curves are more conveniently calculated in parametric form, using the kinetic energy per nucleon (ε) of the incident ion as the parameter on which both S and G depend. In fact, from equation 1.4, and taking into account equation 1.3, if the charge Z (and mass) of the incoming ion is fixed, the reduced etch rate S depends only on the velocity β of the incident ion, and therefore on its kinetic energy per nucleon ε ($S_Z(\varepsilon)$). Similarly, as inferred from equation 1.5, the fractional gradient of reduced etch rate G also depends on this kinetic energy ($G_Z(\varepsilon)$). Consequently, $G_Z(\varepsilon)$, and $S_Z(\varepsilon)$ may be calculated for every fixed charge using ε as a parameter, and the corresponding $S_Z(G)$ curve can be plotted.

$S_Z(\varepsilon)$ is directly calculated using equations 1.4 and 1.3, whereas equation 1.5 has been conveniently transformed by means of the chain rule of derivation and, taking into account equation 1.4, in order to facilitate the calculation of the values of reduced etch rate fractional gradient $G_Z(\varepsilon)$ for a given charge:

$$G \equiv \frac{1}{S}\frac{dS}{dx} = -\left(\frac{h}{REL_{\omega_0}}\right) \cdot \left(\frac{d\left(REL_{\omega_0}\right)}{dE}\right) \cdot \left(-\frac{dE}{dx}\right) \tag{1.8}$$

In this equation, the first term $\left(\frac{h}{REL_{\omega_0}}\right)$ is calculated analytically from equation 1.3 for a given value of the ion kinetic energy $E = A\varepsilon$ (A is the mass number of the ion considered); the second term $\left(\frac{d\left(REL_{\omega_0}\right)}{dE}\right)$ is in practice evaluated by numerical derivation of equation 1.3 at a given value of energy E; and the third term $\left(-\frac{dE}{dx}\right)$ is determined from the Bethe-Bloch energy-loss equation at a given E. The $G_Z(\varepsilon)$ curve is generated by varying the values of energy per nucleon ε at which all these terms are evaluated. In summary, both $G_Z(\varepsilon)$, and $S_Z(\varepsilon)$ may be calculated for every fixed charge using ε as a parameter, and the corresponding $S_Z(G)$ curve can be plotted in the $G-S$ plane.

In all this process, the values of the parameters g and h which characterize the detector response are needed in order to generate these $S_Z(G)$ curves. These values should be obtained from calibration of the SSNTD detectors in accelerators to ions belonging to the same charge and energy region than those recorded in the experiment being analysed.

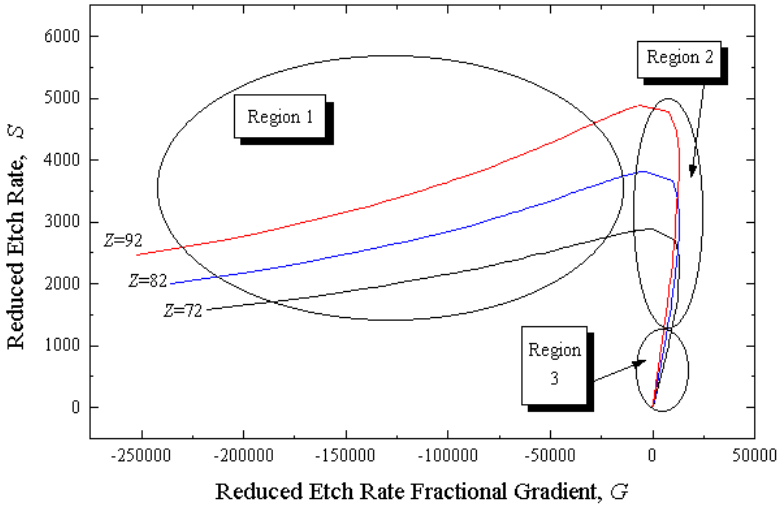

Figure 1.17. $S_z(G)$ curves corresponding to several ions ($Z = 72$, 82 and 92) for an incident energy range of 0.1 MeV/n up to 5000 MeV/n. The three separated regions in which the applicability of the RERFG method is discussed are also illustrated.

Range of applicability

In order to obtain information about the range of validity of the RERFG method a study of the behaviour of the $S_Z(G)$ curves for a wide interval of kinetic energy per nucleon ε has been performed, as ε is the parameter which has been used for generating the $S_Z(G)$ curves. For carrying out this study, incident ion charges in the Ultra Heavy region ($65 < Z < 92$) have been considered. The $S_Z(G)$ curve for each of these charges has been generated by varying the incident ion energy per nucleon ε from 5000 MeV/n down to about 0.1 MeV/n, in order to reproduce the slowing down of a typical ion recorded in the UHCRE detectors. The values of the g and h parameters have been obtained from adequate calibration (see section 1.3.3.). Ranges of 5000 MeV/n ions in the studied charge region lie between 50 to 75 cm in polycarbonate detectors, such as those used in the UHCRE. Figure 1.17 shows the $S_Z(G)$ curves for $Z = 72$, $Z = 82$ and $Z = 92$ (other charges are not displayed for clarity, but the behaviour of the corresponding curves is easily inferred from the figure). For a more detailed study, we have divided the graphs in figure 1.17 into three regions, according to the three different behaviours displayed by the energy deposition of the incoming ion. In addition, figure 1.18 displays an amplification of region 3, which at the same time includes a further amplification of the higher energy end.

Generally speaking and at first sight, the most prominent (and weird) feature of figure 1.17 is that G and S are not uniquely related for a given charge (there is not a one to

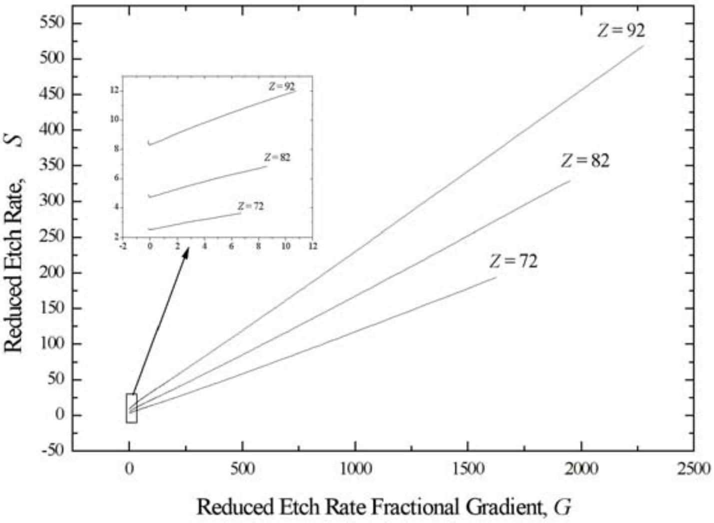

Figure 1.18. $S_Z(G)$ curves corresponding to the same ions than figure 1.17 showing the details of region 3, with a zoom in of the higher energy tail.

one correspondence between G and S). A further complication appears in region 2, where the curves corresponding to different charges cross each other, so that we cannot assign a unique charge value to a given point on the $G-S$ plane. Nevertheless, a closer analysis of figure 1.17, allows to extract valuable information from the graphs. The REL curves as a function of ε for Z = 72, Z = 82 and Z = 92 are plotted in figure 1.19, including an amplification near the stopping point of the incident ion, for clarifying the behaviour in the above regions, which are numbered from low to high energy of the incident ion. These curves are related to the well known Bragg curves, which plot the stopping power as a function of the penetration distance. Figure 1.19 and figure 1.17 are, in fact, closely related: one can convert from figure 1.19 to figure 1.17 for any given (fixed) charge by taking into account that S is directly related to REL by means of equation 1.4, whereas G is related to the slope of the REL curve at the given value of ε.

The main features of each of the three regions in which the $S_Z(G)$ curves has been divided are:

Region 1. For low energies of the incident ion REL increases dramatically with energy until a maximum is reached, related to the Bragg peak. This region includes the largest negative G values in figure 1.17, as inferred from the term $\left(\frac{d\left(REL_{\omega_0}\right)}{dE}\right)$ of equation 1.8. It must be emphasised that although this region is very large in the G-S plane, it corresponds to a very small interval of energies (from 0.1 to 1 MeV/n) of the incoming

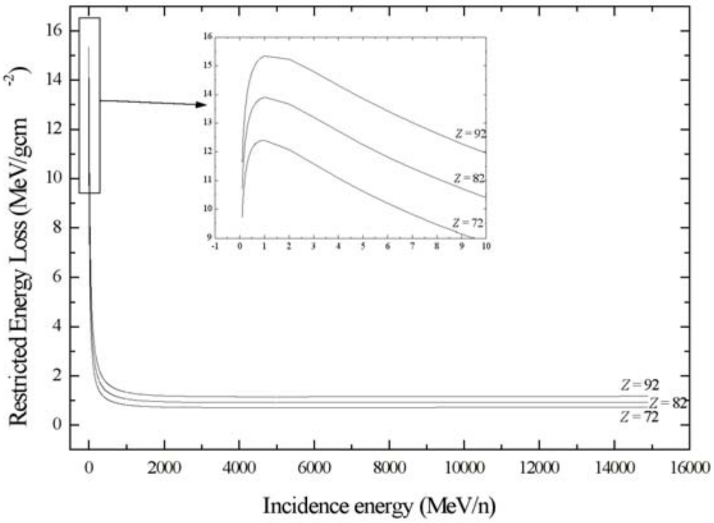

Figure 1.19. Bragg curves for several ions (with charge, $Z = 72$, 82 and 92) with an incident energy of 0.1 MeV/n up to 5000 MeV/n. A zoom of the Bragg curves for the lowest energy region is also plotted in order to evidence the so-called Bargg peak

particle, when it almost completely stops inside the absorber. In terms of ion ranges in the absorber, this region represents approximately the last 20 to 30 mm of the incoming ions total range (a fraction of about 10^{-5}).

Region 2. *REL* decreases with increasing energy, so that in this region the slope of the $\frac{dE}{dx}$ curve is negative and, therefore, G is positive and attains its maximum value. Each curve cross all others in this zone, implying that there are points in the *G-S* plane common to, at least, two charges. The reason for this behaviour is that, for every given pair of charges, there is a unique value of *REL* where their corresponding $\frac{dE}{dx}(\varepsilon)$ curves display exactly the same slope. This region corresponds to an energy interval ranging from about 1 MeV/n to approximately 50 MeV/n for the considered charges, which is equivalent to the last millimeter of the incident ion range (still a fraction of only 10^{-3} of its total range).

Region 3. In this zone, *REL* is almost flat (independent of the ion incident energy), so that the slope of the $\frac{dE}{dx}(\varepsilon)$ curve corresponding to any of the considered charges is very close to zero and, therefore, the associated G values are also close to zero. In this region, the minimum of ionisation is reached, so that for very high energies (above several GeV/n) there is a slight increase of *REL* with energy, and consequently the associated G values are again negative, but small in absolute value. Although this region is the smallest one in the *G-S* plane, the energy interval covered is the widest one, as in principle any energy above 50 MeV/n is included on it. Figure 1.17 displays energies up to 5000 MeV/n, but no relevant change of behaviour is expected for higher energies. In terms of range, this region covers the whole path of any ion of the studied charge interval with the exception of approximately its last millimeter.

From observation of figure 1.17, and taking into account the above comments for each region, it is obvious that the RERFG method is not applicable at all in region 2 for ion identification purposes. In consequence, the method, in principle, might be applied for identifying ions which energy, while slowing down in a given absorber, falls entirely either in region 1 or in region 3. Note that RERFG cannot be applied for identifying high energy (above 50 MeV/n) incoming ions which come into rest inside the detector as, while moving along their path and decreasing their kinetic energy, this energy would fall sooner or later in the interval corresponding to region 2. In addition, in practice, for applying RERFG to identify ions having their energy entirely in region 1 (smaller than 1 MeV/n), it would be necessary to perform several measurements of track geometry along a path smaller than ∼20 μm. This practice is not feasible in a real experiment as plate thickness in SSNTD's stacks are typically of the order of 100 μm. This leaves out region 3 as the only one where the RERFG method is fully applicable. Consequently, this method is convenient for identifying ions that do not reach an energy below about 50 MeV/n in any point along their path inside the absorber and, consequently, that do not halt in it.

The identification of the ions recorded in the UHCRE is a good example where the RERFG method is applicable. In fact, given the thickness of the plastic detector stacks utilised ($\sim$ 4-6 g/cm^2) and the incidence energy of the cosmic ray ions (over ~3 GeV/n), the recorded ions do not come to rest while traversing the detector stacks, thus the conditions of region 3 are completely fulfilled.

Sources of uncertainty

In order to determine the uncertainty on charge introduced by the application of the RERFG identification method, two main sources of uncertainty have to be taken into account. On one hand, the experimental uncertainty which arise from the propagation of the instrumental uncertainty of the track geometric measurements. On the other hand, a "theoretical" uncertainty in the $S_Z(G)$ curves, due to the fact that each of such curves is determined, in essence, from the Bethe-Bloch equation which remains as an "open" expression for the energy loss per unit of length in the sense that its applicability to heavy nuclei with energies above 3 GeV/n is not well known, so that new corrections are still added. For such reason, this "theoretical" uncertainty becomes complex to evaluate and it is not considered in this work.

From the instrumental uncertainty of the geometric measurements, the uncertainty of the reduced etch rate σ_{S_i} is calculated. So that each value of S_i is accompanied by its corresponding σ_{S_i}. The values of $S_i \pm \sigma_{S_i}$ and $x_i \pm \sigma_{x_i}$ are used to evaluate the uncertainty of S_{eff} and G_{eff} (respectively $\sigma_{S_{eff}}$ and $\sigma_{G_{eff}}$) by means of the uncertainty propagation formula applied to the expressions 1.7 and 1.6 which are adequately modified in order to easily perform the partial derivatives. Each recorded nuclei is characterized by S_{eff}, G_{eff} which is situated in the S-G plane. An ellipse taking the $\sigma_{S_{eff}}$ and $\sigma_{G_{eff}}$ values for the respective vertical and horizontal semi-axis is drawn around the experimental S_{eff}, G_{eff} point. Finally, charge uncertainty, σ_Z, is estimated taking into account that it is lineally proportional to the vertical semi-axis value, $\sigma_{S_{eff}}$, and considering that the value of $\sigma_Z = 1$ corresponds to the vertical shift at the S_{eff}, G_{eff} point between the two successive $S_Z(G)$ curves where this point (S_{eff}, G_{eff}) lies between.

1.3.3. Application to the ions recorded in the UHCRE

After the LDEF recovery from Earth's orbit in 1990, the UHCRE was disassembled in the ESA ESTEC. The SSNTD stacks from the UHCRE were sent to the *Dublin Institute for Advanced Studies*, where they were dismounted and their polycarbonate plates taken apart and etched. Our group (*Grup de Física de les Radiacions*, GFR) performed some of the scanning for locating events and geometry measurements of etched tracks. A total of over 2500 tracks originated by UHCR ions have been recorded in the UHCRE, [Osu95a], [Bea95], [Osu95b] & [Osu95c], of which 205 have been located, measured and positively identified as originated by UHCR nuclei with energies over 3 GeV/n by the GFR [Dom95].

It is known that some environmental parameters can affect track registration. In particular, the track response of a SSNTD is known to decrease with increasing registration temperature (the so-called Registration Temperature Effect or RTE) for strongly ionizing particles and seems to increase with temperature for weakly ionizing particles [Tho86]. Pressure and/or oxygen concentration at the moment of track registration can also affect the polycarbonate detector response (the so-called Latent Track Intensification effect, LTI, see [Dom86], [Dom90] and references therein for details). The successful control of both the pressurized gas environment and the temperature through out the mission has led to justified optimism concerning the high quantity of the UHCRE cosmic ray data and the possibility of good charge resolution [Dom90], [Osu95b].

Given the charge and energy of the recorded ions, and as the thickness of the UHCRE stacks (~ 4 to 6 g/cm^2) is much smaller than their range in the detectors, none of such ions come to rest inside the detector. Consequently, residual ranges of such ions cannot be measured and the method based on the R-S relationship is not suitable for identification of ions recorded in UHCRE. In this case, it may be considered as a first approximation that the velocity β of a given ion does not vary substantially while passing through the detector. Therefore, the specific energy loss of the recorded ions should remain almost constant along their path. Geometry measurements of the etched-cone pits have been made using a Nikon stereo-microscope, with eyepieces of 10× or 15× and a long-working distance (1 mm) dry ×100 objective, and with digitized x-, y-, and z- axis measurement outputs connected to a computer. Results obtained from measurements of UHCRE tracks confirm that variations of S along a given track are very small (the bulk etch rate have been performed in about

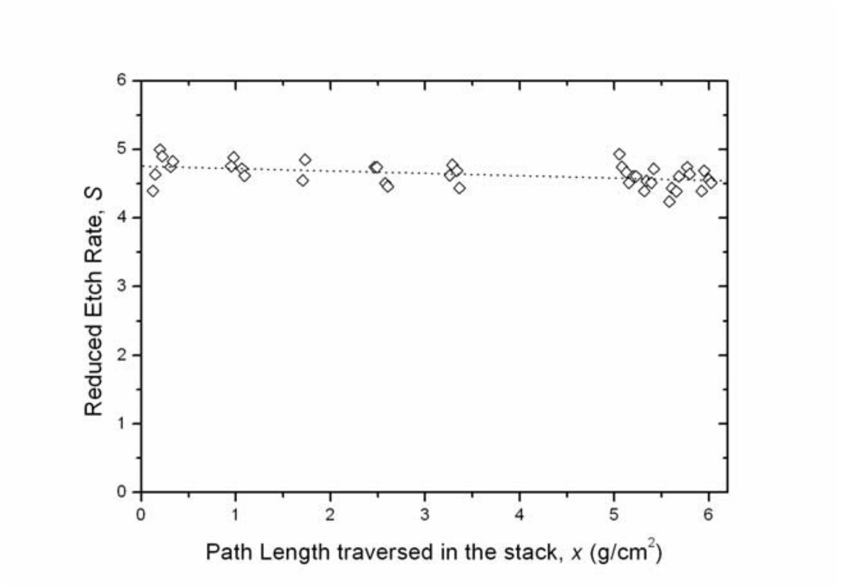

Figure 1.20. A reduced etch rate (S) versus path length (x in g/cm^2) plot of an ultra heavy cosmic ray nucleus recorded in a plastic detector stack of the UHCRE measured in our group.

40 points for each located track, so that each track is characterised by about 40 S_i values) [Kea95], and therefore, in a first approximation, it is correct to represent one track by its corresponding average S value. In consequence, the method based on the averaged S value, described above, can be used. Results using this identification method were presented elsewhere [Font94], [Dom95] & [Dom96].

Although the method described above provides good first approximation results, they may be improved applying the RERFG identification method. In fact, this method is fully applicable in this case as the incident particle transfers a small amount of its kinetic energy to the absorber, which leads to a measurable variation of the incident particle kinetic energy, and therefore $\frac{dS}{dx} \neq 0$, as can be seen in figure 1.20 where the reduced etch rate (S) versus path length (x) is plotted for one UHCR nuclei recorded in UHCRE. So that the conditions of region 3 from figure 1.17 are fully fulfilled.

Bulk nuclei recorded in the UHCRE survive after passage through all plates of the stack, so (S_i, x_i) measured values of its track could be pretty well fitted by a linear function as can be seen in figure 1.20, but not all recorded nuclei follow this behaviour. Some nuclei has been found broken along its path through the stack due to a collision with an atomic nuclei of the traversed material. Probably the fragmentation of the penetrating nuclei would take place in the lead plate of the stack instead of the plastic plate as the cross section for a nucleus-nucleus reaction is, as a first approximation, proportional to $A^{\frac{2}{3}}$ (where A is the mass number of the target nucleus). Figure 1.21 shows a fragmented track of a recorded

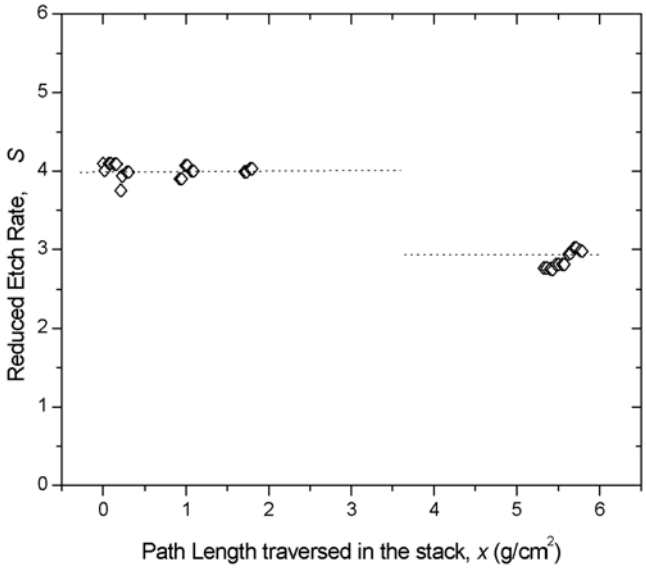

Figure 1.21. Fragmented track of a nuclei recorded in UHCRE. Dotted lines show the mean values of each set of data.

nuclei, the two sets of experimental data are clearly apart, the higher S value corresponds to the penetrating nuclei whereas the lower S value corresponds to the product nuclei.

In order to complete the application of the RERFG identification method it is necessary to know beforehand the values of the parameters g and h that characterise the detector response (equation (4)). Calibration in accelerator of detectors having the same characteristics than those used in the experiment is the usual procedure that allows to determine these values [Kea95]. The values for these parameters $g = 8.02$ and $h = 2.457$ were obtained from a calibration based on exposures of SSNTD's plates at the Berkeley Bevalac heavy ion accelerator to U and Au ions of approximately 1 GeV/n [Dom88], [Dom86] & [Bai91]. Figure 1.22 shows the (S_{eff}, G_{eff}) points obtained for the 205 UHCRE tracks measured by our group, together with some of the most representative $S_Z(G)$ curves in the studied charge region determined from the above accelerator calibration. Once these values are known, the identification process is carried out as described above. Two relevant features are found:

a) All ions recorded in the UHCRE detectors have charge comprised between 65 and 92 ($65 < Z < 92$).

b) The accumulation of the experimental points around the curves corresponding to two distinct charges, namely $Z = 73$ and $Z = 78$.

It is known that UH nuclei ($65 < Z < 92$) can be synthesised in the Universe only

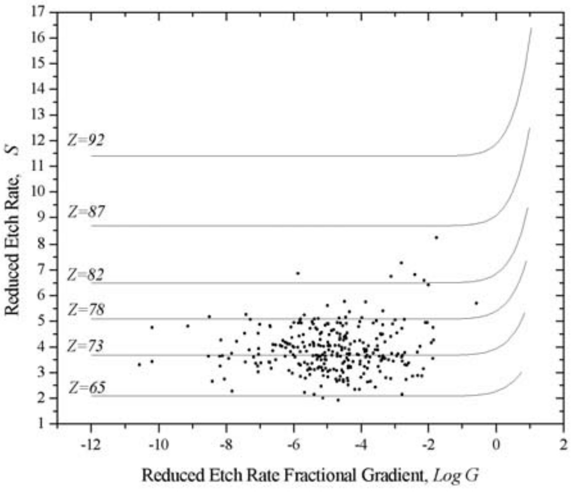

Figure 1.22. Experimental (S_{eff}, G_{eff}) points, in semilogarithmic scale, corresponding to the 205 UHCRE events measured by our group. Also plotted are the $S_Z(G)$ curves for some charges (Z=65, 73, 78, 87 and 92) calculated using the g and h parameters obtained directly from accelerator calibration.

by neutron capture processes. It is possible to distinguish between rapid neutron capture, r-process, and slow neutron capture, s-process, when comparing the time scale of the process with the half-life for β-decay of the newly formed nuclei. As a consequence of these processes two abundance peaks, one corresponding to the Platinum group ($Z = 78$), synthesised mainly by the r-process, and the other one to the Lead group ($Z = 82$), synthesised mainly by the s-process, are present in the UH charge region [Tho87], [Dom87a]. The existence of these two peaks has been experimentally confirmed by previous experiments, such as HEAO-3 and Ariel VI (see references given for such experiments in subsection 1.1.1.). From experimental data presented in figure 1.22 we can conclude that our charge scale is shifted with respect the theoretical predictions by about 4 or 5 charge units.

This discrepancy between our results and the theoretical predictions is explained if the g and h parameters are energy-dependent. The energy of the ions used in the Bevalac accelerator for calibration is about 1 GeV/n, corresponding to $\beta \simeq 0.87$, whereas the energy of ions recorded in the UHCRE are over 3 GeV/n (β over 0.95). It is seen in figure 1.23 that the calibration region and the cloud of UHCRE experimental points are clearly apart from each other, so that probably the values of the parameters obtained from calibration may not be suitable for our case. As no accelerator calibration at UH ions of the appropriate energies of detectors similar to those used on the UHCRE was available, we had to calibrate on the basis of the theoretically predicted position of the abundance peaks in the UH region

($Z = 78$ and $Z = 82$). By doing so, new values of the g and h parameters have been obtained that should allow to correctly apply the RERFG method of identification to the ions recorded in the UHCRE. The newly calculated values of the parameters are $g = 5.807$ and $h = 2.466$ [Font94]. The difference between these new values and the old ones is almost completely due to the multiplicative g parameter and not to the exponent h. As the reduced etch rate fractional gradient G depends only on the value of h for a given ε (see equation 1.8), the fact of re-calibrating has only effect on the values of signal strength S, changing the relative separation of the $S_Z(G)$ curves. The dotted curves in figure 1.23 are the G - S curves corresponding to several UH charges obtained directly from accelerator calibration, strictly valid only in the calibration region in the figure. Conversely, the solid curves are generated taking into account the g and h parameter values calculated from the peak calibration. Such values are valid only in the region of the cloud of experimental points. For any other region in the G - S plane the $S_Z(G)$ curve should fall between the dotted and solid curves corresponding to the desired charge, and the corresponding values of g and h would be comprised between the 'old' and 'new' values of the parameters. This is a clear indication of the fact that the response of the detectors, characterised by the g and h parameters, depends on the incident particle energy and, of course, the most correct procedure to characterise this response is calibration at the adequate energies. Nevertheless, an approximation of the g and h values at any energy may be calculated by appropriate interpolation.

The study of the intrinsic charge uncertainty introduced by the RERFG identification method as described in section 1.3.2. has led a value of $\sigma_Z \simeq 0.1\ e$. This result represents a very low contribution to the expected charge uncertainty for the nuclei recorded in the UHCRE which is estimated to fall in the interval $1.5 - 2\ e$, as already predicted in former works [Dom90]. Figure 1.24 shows the ellipse, generated from the uncertainties $\sigma_{S_{eff}}$ and $\sigma_{G_{eff}}$, which is centered in the S_{eff}, G_{eff} point characterizing a chosen track. The two closest $S_Z(G)$ curves to the experimental point (S_{eff}, G_{eff}) are also plotted in the figure. Results obataines for other tracks display the same behaviour.

1.4. Abundances of Ultra Heavy Cosmic Ray Nuclei recorded in UHCRE

The abundance histogram of the ions recorded in the UHCRE is obtained using the 'new' g and h values and applying the RERFG method. This histogram is displayed in figure 1.25 .Also shown in this figure is a gaussian fit of the peaks observed which are in agreement with the predicted ones in this charge region (*i.e.* the Platinum and Lead abundance peak). The Platinum peak has an area larger than the Lead one, thus indicating an overabundance of the r-synthesised material with respect to the s-synthesised material that reaches the Earth's neighbourhood. In order to derive the appropriate astrophysical implications from this result, it is necessary to determine the cosmic ray source abundances

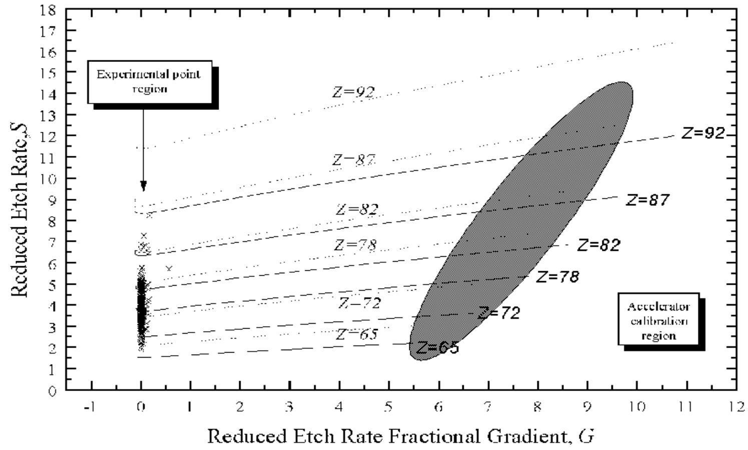

Figure 1.23. $S_z(G)$ curves corresponding to several UH charges using the 'old' values of the g and h parameters obtained from Bavalac accelerator calibration (dotted curves) as well as the 'new' values of these two parameters obtained from our calibration (solid curves). The calibration region with accelerator and the cloud of experimental points are also displayed.

by means of a suitable model of cosmic ray propagation in the Galaxy. On the other hand, although the statistics available for the highest charges is low, a less abundant peak appears for $78 \leqslant Z \leqslant 92$, which is certainly disconnected from the Platinum and Lead peaks. This could be the so-called 'actinide peak', which is the third peak predicted in the UH charge region, according to the neutron capture processes of nucleosynthesis. Results coming from the UHCRE detectors analysed by other groups would provide enough events in this region of highest charges in order to confirm statistically the existence of the actinide peak. It has been observed that no significant variation appears in comparison with the charge histogram obtained applying the approximation of β constant [Dom96]. The results are compatible with charge uncertainty comprised between ~ 1.5 and 2 charge units, as already predicted in former works [Dom90].

Binns [Bin88] defines two abundance ratios in the $Z > 65$ region:

$$R_1 = \frac{Actinide\ abundance\ \ (87 \leq Z\ \ \leq 100)}{Lead + Platinum\ group\ abundances\ \ (74 \leq Z\ \ \leq 86)}$$

$$R_2 = \frac{Lead\ group\ abundance\ \ (81 \leq Z\ \ \leq 86)}{Platinum\ group\ abundance\ \ (74 \leq Z\ \ \leq 80)}$$

In addition, Klarmann *et al* [Kla85] defines a third abundance ratio in the same charge region:

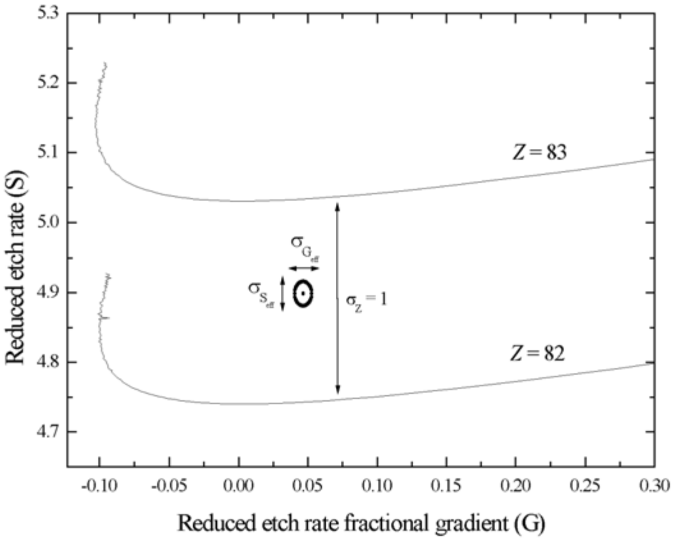

Figure 1.24. Uncertainty ellipse constructed with the values of $\sigma_{S_{eff}}$ and $\sigma_{G_{eff}}$ drawn around the experimental S_{eff}, G_{eff} ponts which is located in the center of the ellipse. The "theoretical" $S_{82}(G)$ and $S_{83}(G)$ curves are also plotted.

$$R_3 = \frac{Abundance\ of\ elements\ with\ \ (70 \le Z\ \ \le 73)}{Lead + Platinum\ group\ abundances\ \ (74 \le Z\ \ \le 86)}$$

Table 1.1 shows the results obtained for R_1, R_2 and R_3 from our data measured in the UHCRE stacks compared to those obtained by other authors in other experiments. Our results are compatible with those obtained by combining the Ariel VI and the HEAO 3 results (the other experiments that were able to separate the Lead and Platinum groups). Comparing values of R_1, R_2 and R_3 in table 1.1 with those corresponding to Solar System abundances proposed by different authors (see table 1.2), the overabundance of r-process synthesized material in the $Z > 65$ region is confirmed, as already stated by other authors [Sch72], [Bin82], [Bin85], [Bin89], [Fix83], [Gil85], [Mar85], [Sto87]. Our value of R_3 however is extremely low compared to those obtained by other authors, but this could be explained by the registration threshold of our detector, that led to a low-registration efficiency for incident ions in the charge range $70 \le Z \le 73$.

1.5. Discussion and conclusions

This chapter has been focused on the study of the Reduced Etch Rate Fractional Gradient (RERFG) identification method and its application to the nuclei recorded in

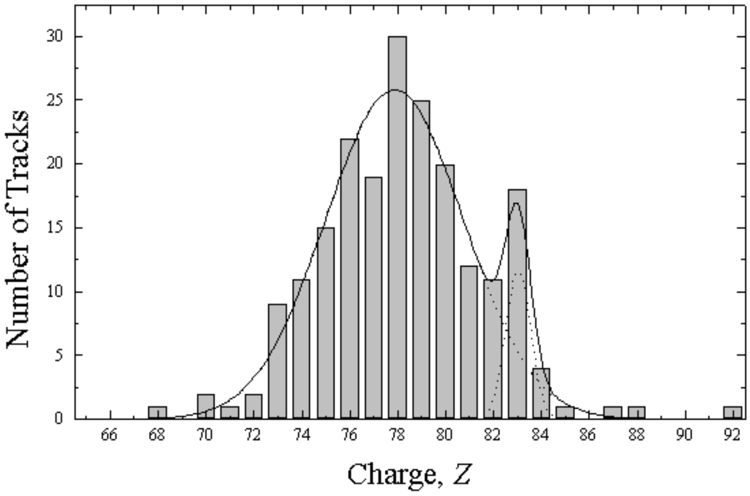

Figure 1.25. Charge histogram corresponding to the 205 UHCR events with $Z > 65$ studied in this work obtained using the method based on the reduced etch rate fractional gradient, the corresponding gaussian fit is also displayed.

UHCRE experience. From the results obtained in this work we may conclude that, in order to identify UH charged particles recorded in plastic track detectors, the RERFG method is fully applicable only for incident ions of kinetic energy over 50 MeV/n which do not come to rest in the detector, the so called region 3 in figure 1.17. In terms of range, this region covers the whole path of any ion of the studied charge interval with the exception of approximately its last millimeter. This method is fully applicable to UH nuclei recorded in the UHCRE, and the results of charge identification of the recorded nuclei are in agreement both with the theoretical predictions [Tho87], [Dom87a] and with previous results from other experiments [Shi78], [Bin89] & [Fow87].

Nevertheless, several problems arise in practice when the RERFG method is applied. Probably, the most important of them is the fact that the detector response is only characterised through a model (*REL* model) that was first developed for incident ions of smaller charges and energies than those we are dealing with. There is clear indications that the parameters on which the detector response depends (g and h) are energy and may be charge dependent, evidencing either the limitations of the track formation model itself or the non-ideal behaviour of the detector. Certainly, the fact of calibrating from accelerator data has allowed us to evidence the non-validity of accelerator calibration in a different energy region (the region of experimental points), thus showing that the g and h parameters

Table 1.1. Abundance ratios R_1, R_2 and R_3 calculated from several experiments by different authors, including our UHCRE results.

	Ariel VI	HEAO-3	Combined Ariel + HEAO-3	*UHCRE*
R_1	0.04	0.010	0.024	0.016
R_2	0.35	0.25	-	0.32
R_3	0.16	0.27	-	0.074

Table 1.2. Coefficients R_1, R_2 and R_3 calculated from several Solar System abundances, including an r-process source one.

	SS [Cam82]	SS [And82]	SS [And89]	r-source [Bin85]
R_1	0.011	0.006	0.006	0.013
R_2	0.816	0.936	1.026	0.596
R_3	0.065	0.068	0.067	0.060

display a "*local*" behaviour. These parameters should depend, on the ideal case, only on the detector characteristics. In this work, the model has been applied '*locally*', as values of g and h have been calculated for the energies of the ions involved, and is valid only for these energies. For any different range of energies, different values of the parameters must be determined, as it has been done in this work when a 'new' calibration has been performed in order to reproduce the correct charge scale. In the case that a '*global*' (as opposed to '*local*') treatment of the detector response is to be carried out, it would be necessary to determine the dependence of g and h with energy, either by analytical calculation of $g(\varepsilon)$ and $h(\varepsilon)$, if possible at all, or by adequate interpolation between known values. If this was the case, expression 1.8 should be conveniently modified, as it has been developed assuming that g and h are constant.

On the other hand, the identification method is based on the track formation model and, therefore, on the energy deposited by the incident charged particle in the detector, ruled by the Bethe-Bloch equation. The incident particle charge and energy values for which the Bethe-Bloch equation is applicable [Fan63], are limited [Nor63], so that several corrections, in addition to the shell correction and the density effect correction already taken into account in the 'uncorrected' formula, should be introduced if UH ions of high energies, such as those recorded in the UHCRE, are considered [Osu88]. The effect of the quantic Bloch, the relativistic Bloch, the Mott, and the Leung corrections should be considered, as other corrections which only contribute to stopping power for low or very low velocities of the incident particle may be neglected for high energies. The last correction introduced in the stopping power (Bethe-Bloch) formula [Lin96] appears when nuclear size effects are taken into account. Consequently, this correction has an important contribution for high energies and high atomic numbers of the penetrating particles [Dat96]. All these corrections may be included in a 'corrected' Bethe-Bloch equation.

A charge histogram of the abundances near the Earth's neighborhood of UH cosmic ray ions with $Z > 65$ recorded in the UHCRE has been obtained using a charge identification method based on the fractional gradient of the reduced etch rate together with the *REL* criteria as a latent track formation model. The energy dependence of the parameters g and h has forced us to refuse the calibration made in the Berkeley Bevalac accelerator at an energy $\lesssim 1$ GeV/n, because the energies of the ions recorded in the UHCRE detectors are $\gtrsim 3$ GeV/n. In our case a calibration based on the knowledge of predicted peaks have been applied.

The UH cosmic ray composition seen by the UHCRE detectors shows the existence of two separate abundance peaks. The Platinum group peak consisting of rapid neutron capture process synthesized elements which is the most abundant, and secondly the Lead group peak which is composed of slow neutron capture process built up elements. Both peaks are also present in the Solar System abundances but with a different ratio. This behavior is reproduced when the measured composition from other experiments (mainly, Ariel VI and HEAO 3) is compared to the Solar System one. These differences between the Solar System abundances and the measured ones, can be justified if the production of secondary elements by nuclear interaction (mainly spallation) with the interstellar medium Hydrogen through the propagation process is considered.

The study of the charge uncertainty introduced intrinsically because of the application of the RERFG method to the nuclei detected by the SSNTD's used in the UHCRE has revealed that this identification method is not the main source of uncertainty; $\sigma_Z \simeq 0.1$ e whereas the charge resolution for the UHCRE detectors is estimated to be $\simeq 1.5 - 2e$. Thus, in order to justify the expected charge resolution, all other uncertainty sources have to be taken into account, as uncertainty introduced by the Bethe-Bloch equation, the influence of the RTE and the LTI effects.

References

[Ahl82] S.P. Ahlen, Phys. Rev. **25** (1982) 1856.

[And82] E. Anders and M. Ebihara, Geochim. et Cosmochim. Acta **46** (1982) 2363.

[And89] E. Anders and N. Grevesse, Geochim. et Cosmochim. Acta **53** (1989) 197.

[Bai91] C. Baixeras *et al.*, Nucl. Tracks and Rad. Meas. **19** (1991) 675.

[Bea95] R. Beaujean *et al.*, Rad. Meas. **25** (1995) 325.

[Ben68] E.V. Benton & R.P. Henke, Nucl. Instr. and Meth. **58** (1968) 241.

[Ben69] E.V. Benton & W.D. Nix, Nucl. Instr. and Meth. **67** (1969) 243.

[Ber97] V. Berezinsky, talk given at the workshop "Observing the Highest Energy Particles from Space" (Maryland, 1997).

[Bin82] W.R. Binns et al. Astrophys. J., **261** (1982) L117.

[Bin85] W.R. Binns *et al.*, Astrophys. J., **297** (1985) 111.

[Bin88] W.R. Binns, Genesis and propagation of cosmic rays, M.M Shapiro & J.P. Wefel eds. (D. Reidel, 1988) p.71.

[Bin89] W.R. Binns *et al.*, Astrophys. J., **346** (1989) 997.

[Bin95] W.R. Binns, Adv. Space Res., **15** (1995) 29.

[Bin97] W.R. Binns *et al.*, Proc. 25th Int. Cosmic Ray Conf. (Durban, 1997), OG 10.2.16.

[Boo97] K. Boothby *et al.*, Astrophys. J., **491** (1997) L35.

[Cam82] A.G.W. Cameron, Essays in Nuclear Astrophysics, C.A. Barnes et al., eds. (Cambridge Univeriity Press, 1982) p. 23.

[Dat96] S. Datz *et al.*, Phys. Rev Lett. **77** (1996) 2925.

[Dom86] C. Domingo *et al.*, Nucl. Tracks **12** (1986) 395.

[Dom87] C. Domingo *et al.*, Proc. 20th Int. Cosmic Ray Conf. (Moscow, 1987), vol. **2**, p.406.

[Dom88] C. Domingo, Ph. D. Thesis (Universitat Autònoma de Barcelona, 1988).

[Dom90] C. Domingo *et al.*, Nucl. Instr. and Meths. **B 51** (1990) 253.

[Dom95] C. Domingo *et al.*, Proc. 24th Int. Cosmic Ray Conf. (Roma, 1995), vol. **2**, p.572.

[Dom96] C. Domingo *et al.*, Rad. Meas. **26** (1996) 825.

[Dur87] S.A. Durrani & R.K. Bull, Solid state nuclear track detection. Principles, Methods and Applications, ed. (Oxford, Pergamon, 1987)

[Erl01] A.D. Erlykin & A.W. Wolfendale, Proc. of rencontres de Morimond (Les Arcs, 2001).

[Fan63] V. Fano, Ann Rev. Nucl. Sci. **13** (1963) 1.

[Fer81] F. Fernandez *et al.*, Proc. 11st Int. Conf. SSNTD's (Bristol, 1981) p. 261.

[Fix83] D.J. Fixen *et al.*, Proc. 18th Int. Cosmic Ray Conf. (Bangalore, 1983), vol. **9**, p.119.

[Fle75] R.L. Fleischer *et al.*, Nuclear tracks in solids. Principles and Applications, ed. (Universitu of California Press, 1975) p. 166.

[Font94] J. Font, Ms. Sc. Thesis (Universitat Autònoma de Barcelona, 1994).

[Fow77a] P.H. Fowler, Proc. 19th Int. Conf. SSNTD's (Munich, 1977) p. 983.

[Fow77b] P.H. Fowler *et al.*, Nucl. Instr. and Meths. **147** (1977) 195.

[Fow85] P. H. Fowler *et al.,* Proc. 19th Int. Cosmic Ray Conf. (La Jolla, 1985), vol. 2, p.115.

[Fow87] P. H. Fowler *et al.* Astrophys. J., **314** (1987) 739.

[Gil85] M. Giler & T. Wibig, 19th Int. Cosmic Ray Conf. (La Jolla, 1985), vol. 3, p.17.

[Gre91] J.M. Greenberg, Cosmic Rays, Supernovae and the Interstellar medium, M.M. Shapiro *et al.* eds. (D. Reidel, 1991) p.57.

[Hil72] A.M. Hillas, Cosmic Rays (Pergamon Press Ltd., 1972) p. 9.

[Isb97] J. Isbert, Proc. 25th Int. Cosmic Ray Conf. (Durban, 1997), OG 10.2.14.

[Isr83] M.H. Israel, Composition and origin of Cosmic Rays, M.M Shapiro ed. (D. Reidel, 1983) p. 47.

[Kea95] A.J. Keane *et al.*, Adv. Spa. Res. **15** (6) (1995) 71.

[Kla85] J. Klarmann *et al.*, Proc. 19th Int. Cosmic Ray Conf. (La Jolla, 1985), vol. **2**, p.127.

[Lin96] J. Linhard & A. Sørensen, Phys. Rev. **A53** (1996) 2443.

[Luc82] H.B. Lück, Nucl. Instr. and Meths. **198** (1982) 611

[Mar85] S.H. Margolis & J.B. Blake, Astrophys. J. **299** (1985) 334.

[Nor63] L.C. Northcliffe, Ann. Rev. Nucl. Sci. **13** (1963) 67.

[Ost00] M. Ostrowski, Proc. European cosmic ray Symposium (Lodz, 2000).

[Osu88] D. O'Sullivan *et al.*, Nucl. Tracks and Rad. Meas. **15** (1988) 673.

[Osu92] D. O'Sullivan *et al.*,1st LDEF post-retrival Symposium (1992).

[Osu95a] D. O'Sullivan *et al.*, Rad. Meas. **25** (1995) 295..

[Osu95b] D. O'Sullivan *et al.*, Adv. Spa. Res. **15** (1) (1995) 15.

[Osu95c] D. O'Sullivan *et al.*, Adv. Spa. Res. **15** (6) (1995) 25.

[Pri75] P.B. Price & E.K. Shirk, Proc. 14th Int. Cosmic Ray Conf. (Munchen, 1975), vol. **1**, p.268.

[Ros97] T.T. von Rosenvinge *et al.*, Proc. 25th Int. Cosmic Ray Conf. (Durban, 1997), OG 10.2.20.

[Sch72] D.N. Schramm, Astrophys. J. **177** (1972) 325.

[Seq76] J. Sequeiros *et al.*, Nucl. Instr. and Meths. **135** (1976) 133.

[She85] M.A. Shea & D.F. Smart, Proc. 19th Int. Cosmic Ray Conf. (La Jolla, 1985), vol. **4**, p.501.

[Shi78] E.K. Shirk & P.B. Price, Astrophys. J., **220** (1978) 719.

[Sig01] G. Sigl, Science **291** (2001) 73.

[Sil90] R. Silberberg & C.H. Tsao, Phys. Rep., **191** (1990) 351.

[Spo00] S.H. Sposato *et al.*, Proc. Int. School of Cosmic Ray Astrophys.M.M. Shapiro et al. eds. (World Scientific, 2000) p. 303.

[Ste71] R.M. Sternheimer & R.F. Pierls, Phys. Rev. B **3** (1971) 3681.

[Sto87] E.C. Stone *et al.*, Proc. 20th Int. Cosmic Ray Conf. (Moscow, 1987), vol. **1**, p.366.

[Tho86] A. Thompson *et al.*, Nucl. Tracks **12** (1986) 391.

[Tho87] A. Thompson *et al.*, Proc. 20th Int. Cosmic Ray Conf. (Moscow, 1987), vol. **2**, p.402.

[Tho91] A. Thompson *et al.*, Proc. 22nd Int. Cosmic Ray Conf. (Dublin, 1991), vol. **4**, p.543.

[Tho92] A. Thompson et al., 2nd LDEF post-retrival Symposium (1992).

[Tho93] A. Thompson *et al.*, Proc. 23rd Int. Cosmic Ray Conf. (Calgary, 1993), vol. **1**, p.603.

[Vid84] A. Vidal-Quadras *et al.*, Nucl. Instr. and Meths. in Phys. Res. **223** (1984) 166.

[Wal52] M.C. Walske, Phys. Rev. **88** (1952) 1283.

[Wal56] M.C. Walske, Phys. Rev. **101** (1956) 940.

[Web74] W.R. Webber & J.A. Lezniak, Astrophys. Spa. Sci., **30** (1974) 361.

[Wef88] J.P. Wefel, Genesis and propagation of cosmic rays, M.M Shapiro & J.P. Wefel eds. (D. Reidel, 1988) p.1.

[Wes95] A.J. Westphal*et al.*, Adv. Space Res., **15** (1995) 5.

2. Study of Ultra Heavy Nuclei Latent Track Formation model in Solid State Nuclear Track Detectors

Nature uses as little
as possible of anything

JOHANNES KEPLER

2.1. Introduction

The interest of our research group has been concentrated for several years mainly on passive track detectors and, in particular, on plastic track detectors which are called *Solid State Nuclear Track Detectors* (SSNTD). For instance, this kind of detectors have been used in the *Ultra Heavy Cosmic Ray Experiment* (UHCRE) in order to collect a statistically significant sample of arriving nuclei of $Z > 65$ and energy over ~ 3 GeV/n which belong to the primary cosmic radiation, arriving to near the Earth neighbourhood.

The knowledge of the physical process of energy deposition by the incident particles in the track detectors and of the relationship between the response of the detector and this energy deposition is essential in order to attain precise and reliable results in the work developed. In particular, it is of great importance to fully characterise the particle registration process that takes place into the detector when the charge of unknown ions is intended to be identified.

In summary, the main steps involved in ion registration in tracks detectors and the physical magnitudes related to them are:

- The *Stopping Power* ($\frac{dE}{dx}$) of a charged particle in a given absorber is related to the incident particle characteristics, and specifically to its charge Z and energy E, as well as the absorber characteristics.
- A *Track Formation Model* tells which fraction of $\frac{dE}{dx}$ contributes to the formation of latent tracks in the absorber material. This fraction of the stopping power is the physical quantity characterising the model.
- An *Identification Method* relates, by means of a more or less complex procedure, the physical quantity characterising the track formation model to the recorded signal strength S and allows, finally, to determine the charge and energy of the incident ion.

The main goal of the present chapter is to put forward a new track formation model based on a modification of the known *Restricted Energy Loss* (REL) model which has been applied to identify the nuclei recorded in the SSNTD employed in the UHCRE experience (see chapter 1). The parameters associated to the REL track formation model are energy dependent, as discussed and concluded in the previous chapter. The aim of the proposed track formation model is to study the energetic dependence of such parameters and, thus, make them depend only on the detector characteristics, in the case of eliminating such energetic dependence.

2.2. Interaction of fast heavy ions with matter

A fast heavy charged particle penetrating into matter loses energy predominantly by collisions with the absorber electrons. In this context, a heavy particle is a particle with rest mass much bigger than the electron one. The energy loss of such particles is characterised by the magnitude called *stopping power*, which accounts for the energy deposited in the absorber per unit length $\frac{dE}{dx}$. The stopping power depends on several characteristics of the incident particles (such as their charge and energy) and of the absorber (such as its density, mean atomic number and ionisation potential), and is usually calculated following the Bethe-Bloch formula. In some way, the stopping power is the *"identity card"* of a given particle that enters into a given absorber, in the sense that is the only information that the incident particle can provide. Hereinafter, we will only deal with the particular case of incident heavy charged particles being fully stripped ions, as it is the case of the heavy hadronic component of cosmic rays arriving near the Earth.

The sub-microscopic damage, known as latent track, produced by a fast heavy particle travelling inside a SSNTD is due to the process of energy deposition. Therefore, the latent track damage intensity should be related in some way to the stopping power $\frac{dE}{dx}$. A *track formation model* proposes which fraction of the energy deposited in the absorber is responsible of the latent track formation. Unfortunately, latent tracks are not directly measurable in an easy way, so that it is necessary to perform some etching process (chemical or electrochemical) to make them visible under optical devices, obtaining the so-called etched track. The signal recorded in SSNTDs is usually defined as a function of measurable geometric parameters from the etched track and is characterised by a variable called signal strength (S). With such a definition, there should be a (more or less complicated) relationship between signal recorded and latent track damage intensity. This relationship, together with a suitable procedure for relating the signal strength S to the characteristics of the incident ion, configure the so called *identification method*, as the registered signal strength S carries information about the charge and energy of the recorded ion. Moreover, S may depend not only on the particle and absorber characteristics, but also on the etching process needed in order to visualise the latent track and on other environmental parameters, such as the registration temperature or the oxygen concentration among others as stated in numerous former works [Pri86], [Ada86], [Tho86], [Tho87], [Dom87a], [Dom87b], [Osu87], [Dra87], [Pri87] and [Dom90].

Difficulties arise in practice as none of the three steps quoted above (*i.e.* the stopping power, the track formation model and the identification method) is fully well known. In some cases: *i*) the stopping power expression given by the Bethe-Bloch formula is not fully applicable in the energy range of the studied incident particles, as it is the case of fast heavy ions loosing energy in solid absorbers; *ii*) track formation models are not completely understood; and *iii*) it is difficult to parametrise the variations of S induced by the effects of the etching process on the latent track. These difficulties are normally overcome by means of detector calibration in accelerators to ions of known charges and incidence energies. Calibration allows to assign a relationship between the registered ion charge Z and kinetic energy E and the recorded signal strength S.

2.2.1. The Stopping Power

Energy losses of charged heavy particles are commonly calculated by means of the Bethe-Bloch formula [Fan63], [Nor63] (hereinafter, *uncorrected* Bethe-Bloch formula). In particular, the uncorrected formula is not applicable to fast ions with Z $\geqslant$ 30 due to assumptions and approximations utilized in its mathematical deduction [Ahl80]. In addition, this equation is only strictly valid for rarefied gas absorbers. Several corrections have been introduced in the uncorrected Bethe-Bloch equation in order to extend its range of applicability to a wider range of ion charges and energies as well as absorbers [Ahl80], [Ahl78], [Ahl82], [Ste82], [Gei82], [Leu89], [Bic92] and [Lin96], thus obtaining a *corrected* Bethe-Bloch formula.

The *uncorrected* Bethe-Bloch equation

It is well known that fast heavy particles passing through matter lose energy predominantly by ionisation and excitation of the absorber atoms. Elastic nuclear collisions (i.e. *nuclear stopping power*) are only relevant in the case of calculating the energy loss of an incident heavy charged particle with an extremely low energy ($\beta < \frac{1}{137}$) [Fan63], so that they may be neglected when faster heavy charged particles are considered. Other contributions to the energy loss, such as radiative corrections and spin effects, appear only for heavy charged particles of extremely high velocity. This study is limited to non-ultrarelativistic ions for which radiative and internal structure corrections may be neglected.

In order to quantify the energy loss of a charged heavy particle, the stopping power denoted by $-\frac{dE}{dx}$, is defined as the average energy lost by the particle in the absorber per unit of path length. Alternatively, the stopping power may be written in units of mass thickness $\xi = \rho x$, where ρ is the absorber density, so that $-\frac{dE}{d\xi} = -\left(\frac{1}{\rho}\right)\left(\frac{dE}{dx}\right)$. In order to obtain an expression for the stopping power, several theoretical treatments have been performed, leading to different solutions. All these solutions have a common term (*universal term*) and a dimensionless multiplier, L, called *stopping number.* The general expression for the stopping power may be written as:

$$-\frac{dE}{d\xi} = \frac{4\pi N_A e^4}{m_e}\frac{Z_1^2 Z_2}{v^2}\frac{1}{A}L \tag{2.1}$$

where N_A is the Avogadro number, e is the electron electric charge, m_e is the rest mass of the electron, Z_1 is the electric charge of the incident particle in units of the electron charge, v is its velocity, Z_2 is the atomic number of the absorber, and A is its atomic mass.

Different authors have proposed expressions for the solution to the stopping power equation using different approaches to the theoretical problem. In 1913 and 1915, N. Bohr suggested the following expression for the stopping number [Boh13], [Boh15] applying a classical treatment:

$$L = \ln\frac{1.123 m_e v^3}{Z_1 e^2 \langle\omega\rangle} - \ln\left(1-\beta^2\right) - \frac{\beta^2}{2} \tag{2.2}$$

where $\langle\omega\rangle$ is the geometric mean cyclic frequency of the orbital electrons of the absorber. In the decade of 30's H. Bethe, found a different expression for L [Bet30], [Bet32] after performing a quantic treatment of the problem:

$$L = \ln\frac{2m_e v^2}{I} - \ln\left(1-\beta^2\right) - \beta^2 \tag{2.3}$$

being I the mean excitation energy of the atomic electrons. Afterwards, F. Bloch in 1933 introduced a correction to the former expressions for this term [Blo33] using a combination of classic and quantic treatment:

$$L = \ln\frac{2m_e v^2}{I} + \psi(1) - \operatorname{Re}\psi\left(1+i\nu\right) - \frac{1}{2}\ln\left(1-\beta^2\right) - \frac{\beta^2}{2} \tag{2.4}$$

where $\psi(1) - \mathrm{Re}\,\psi\,(1+iv)$ is the Bloch correction, with ψ the logarithmic derivative of the Euler Γ function, $\psi\,(z) \equiv \frac{d[\ln\Gamma(z)]}{dz}$, and $\nu = \frac{Z_1\alpha}{\beta}$ being $\alpha = \frac{1}{137}$ the structure constant of the electromagnetic coupling. Finally, N. Bohr in 1948 toke up again this question and announced a new expression for the stopping number [Boh48], when combining the classical characteristics of equation 2.2 with the quantic ones of equation 2.3:

$$L = \frac{1}{2}\left\{\sum_s \ln\left(\eta_s^2\,[\varkappa]^{-2}\right) + \sum_s \eta_s^2\left[\frac{\varkappa}{\eta_s}\right]^{-1}\right\} \tag{2.5}$$

with $\eta_s = \frac{2v}{u_s}$, being u_s the orbital velocity of the s-th electron of the absorber, and $\varkappa = \frac{2Z_1v_0}{v}$ where $v_0 = \frac{e^2}{\hbar}$ ($\hbar$ is the Planck constant).

All these solutions have been evaluated using different classic and quantic treatments and separating the contribution of the *close collisions* and of the *distant collisions* to the stopping power. Close and distant collisions may be distinguished, depending on the calculation method, by means of their impact parameter or by the amount of momentum transfer.

As the relativistic extension in the Bohr formula (2.2) and also in the Bloch formula (2.4) is miscalculated because of an incorrect treatment of the close collisions [Ahl80], the Bloch solution to the stopping power, equation 2.4, is combined with the Bethe relativistic extension, in equation 2.3 in order to obtain the known Bethe-Bloch formula for stopping power:

$$-\frac{dE}{d\xi} = \frac{4\pi N_A e^4}{m_e c^2}\frac{Z_1^2 Z_2}{\beta^2}\frac{1}{A}\left[\ln\left(\frac{2m_e c^2}{I}\frac{\beta^2}{1-\beta^2}\right) - \beta^2 + \psi(1) - \mathrm{Re}\,\psi\,(1+i\nu)\right] \tag{2.6}$$

Hereinafter equation 2.6 will be quoted as the *uncorrected Bethe-Bloch formula.*

The *corrected* Bethe-Bloch equation

It is necessary to make several simplifying assumptions and approximations (which can be found summarised in [Ahl80]) in order to deduce the uncorrected Bethe-Bloch formula. For this reason, any calculation carried out using this formula is only approximate. The region of applicability of this formula, with respect to the velocity and the charge of the incident particle as well as the absorber characteristics, is restricted by the validity of the approximations adopted. Various correction terms appear in the Bethe-Bloch formula when different approximations are left to be considered which may be classified into two groups, depending on their contribution to the stopping power for fast heavy charged particles.

i) *Relevant corrections.* These corrections are due to the non-validity of one or several of the following approximations: considering the absorber as a cold diluted gas, considering the finite nuclear size of the incident particle, neglecting the internal structure and the spin of the projectile, neglecting Bremmstrahlung and other radiative phenomena, treating close collisions in the first Born approximation, and the limiting conditions $\gamma \ll$

$\frac{M_{ion}}{m_e}$. Corrections of this group are the density effect (D), the Nuclear Size correction (Δ_{NS}), the Mott correction (M) and the relativistic Bloch correction (C_R).

ii) Negligible corrections. Corrections of this group are due to the non-validity of one or several of the following approximations: considering the projectile velocity much higher than the absorber atomic electrons characteristic velocity, taking into account the projectile charge constant, assuming the dipole approximation for the description of the collisions, and neglecting the relativistic motion of the inner electrons of high Z absorber atoms. The related corrections are: the inner shell correction (S), the effective charge of the incident particle (Z_{eff}) including the gas-solid effect, the low velocity correction (F), and the Leung correction (Δ_R).

The corrected Bethe-Bloch formula which includes the above corrections, allows to extend the range of applicability of the uncorrected formula 2.6, and may be written as:

$$\begin{aligned} -\frac{dE}{d\xi} &= \frac{4\pi N_A e^4}{m_e c^2}\frac{Z_{eff}^2}{\beta^2}\frac{Z_m}{A}\left[\ln\left(\frac{2m_e c^2}{I_m}\frac{\beta^2}{1-\beta^2}\right)\right. \\ &\left. -\beta^2 + B - S - D + M + C_R - \Delta_R + \Delta_{NS}\right]\cdot F \end{aligned} \tag{2.7}$$

were the corrections introduced are described in table 2.1 ,and

Z_m, is the mean atomic number of the absorber.

I_m, is the adjusted ionisation potential of the absorber. Its value may be calculated semiempirically [Ste82], or using the Bragg rule taking into account the chemical structure of the given element in the compound [Ahl80], [Zie88].

Z_{eff}, is the incident particle effective charge in units of the electron charge, given by the semiempirical relation [Bar63], [Pie68], $Z_{eff} = Z_1\left(1 - \exp\left[-130\beta/Z_1^{2/3}\right]\right)$, which does not depend on the absorber. The validity of this relation is limited by the gas-solid effect [Gei82], [Bim92], which makes the effective charge dependent on the absorber characteristics. According to this effect which is relevant only when the incident ion is not fully stripped [Her91], the effective charge is slightly underestimated for slow ions in dense absorbers if the above expression is used.

$B = \psi(1) - \mathrm{Re}\,\psi\,(1 + i\nu)$ is the quantic Bloch correction which already appears in equation 2.6 and is also described in table 2.1.

Strictly speaking, expression 2.7 should, in addition, be multiplied by an extra factor, which sometimes is referred to as Ultrarelativistic correction, and which accounts for the energy loss by bremmstrahlung and not by collisions.

A computer program has been developed for the analytical calculation of the stopping power for any incident fast heavy ion in any dielectric absorber, using the Bethe-Bloch

Table 2.1. Description of the corrections introduced in the uncorrected Bethe-Bloch formula in order to extend its applicability to a wider charge and energy range of the incident heavy charged particles and to a larger number of absorbers.

	Correction	Due to	References	Notes
B	Quantic Bloch correction	Close collisions	[Blo33]	Quantic correction, not valid in the relativistic limit.
C_R	Relativistic Bloch correction	Close collisions	[Ahl82]	Introduced to make B valid in the relativisitic limit. θ_0 and λ are parameters that should be obtained from a semiempirical fit.
S	Inner shell correction	Close & distant collisions	[Bic92]	The correction takes into account that the absorber electrons have finite velocities.
D	Density effect	Distant collisions	[Ste82]	Takes into account the polarisation of the absorber by the incident particle. Appears only for $\beta < 0.85$.
M	Mott correction	Close collisions	[Ahl78] [Ahl80]	Appears when the Mott cross section is consideren instaed of the Rutherford cross section.
Δ_R	Leung correction	Close collisions	[Leu89]	Takes into account the relativistic motion of the inner shell electrons of high Z_2 absorbers.
Δ_{NS}	Nuclear size correction	Close collisions	[Lin96]	Takes into account the finite nuclear size of the incident fast heavy charged particle. Its effect should be relevant when $\gamma A^{1/3} \approxeq 160$.
F	Low velocity correction	Close & distant collisions (each of them contributes half of the correction)	[Ahl80]	This correction, toghether with the Mott correction, accounts the Barkas effect. It has been suggested [Wad86] that considering this correction with the Z_{eff} expression is questionable, as both corrections seem to account for the same physical process.

equation with corrections. It must be emphasised that an analytical calculation has been performed, rather than a semiempirical one or a Monte Carlo transport of particles, as we are interested on the study of the contribution to the stopping power of each term of the corrected Bethe-Bloch equation in order to select those corrections which are relevant for track formation in SSNTD's of ions with charge and energy similar to those recorded in UHCRE.

2.2.2. The Track Formation Model

The Bethe-Bloch formula (in both versions, *i.e.* uncorrected and corrected) allows to calculate the energy loss per unit of path length of an incident heavy charged particle passing through matter, and in particular through SSNTD. A track formation model decides which fraction of the deposited energy inside the SSNTD is invested in damaging the chemical structures of the traversed plastic detector. This damage of submicroscopic size, called *Latent Track*, becomes visible when an etching process is performed to the SSNTD, and hence geometric measurements can be made using an ordinary optical microscope. Actually, a latent track is only formed when the transferred energy per unit of path length exceeds a registration threshold, which depends on the detector characteristics on ideal case. Several track formation models have been developed such as:

The *Total Energy Loss model* [Fle64]. According to this model all energy deposited by the penetrating particle in the plastic detector exceeding the registration threshold is responsible of the latent track formation. The model fails due to it predicts registration thresholds which depend on the matter characteristics and also on the charge of the recorded particle.

The *Ion Spike mechanism* [Fle65]. This model assumes that, along the path of the incident particle, a displacement of the detector electrons is experienced and consequently a cylinder region with positive charge is produced. Net displacements on the plastic detector, which are caused by the electrostatic repulsion between the charged cylinder and the ions of the matter, are responsible of the latent track formation.

The *Primary Ionisation model* [Fle67]. According to this model, which is a modification of the ion spike mechanism, the formation of the latent track is determined by the number of the ions produced per unit of path length along the particle trajectory which is characterized by means of the magnitude $\frac{dJ}{dx}$, instead of the stopping power, which excludes the ionisation originated by secondary particles.

The *Restricted Energy Loss model* (REL) [Ben68], [Ben69]. According to the REL track formation model, the latent track formation is due only to the energy deposited by the distant collisions of the incident particle with the absorber electrons. Distant collisions are defined as those with large impact parameter, originating recoil electrons with low energy (ω), smaller than a fixed value (ω_0) that depends on the absorber, and which deposit their energy in the neighbourhood of the incident particle path. In the derivation of the corrected Bethe-Bloch equation (equation 2.7), the contributions of close (those originating recoils with $\omega > \omega_0$) and of distant collisions are treated separately and subsequently combined to obtain the expression giving the total energy loss of a given ion. This expression is finally independent on ω_0. But, if we are interested on calculating the Restricted Energy Loss (as opposed to total energy loss), the energy transferred from the incident charged particle to the absorber electrons is separated in two parts

$$-\frac{dE}{d\xi} = -\left(\frac{dE}{d\xi}\right)_{\omega<\omega_0} - \left(\frac{dE}{d\xi}\right)_{\omega>\omega_0} \tag{2.8}$$

where the first term corresponds to distant collisions and contributes to latent track formation, and the second one is the close collisions term, not contributing to track formation in the REL model. The corrected Bethe-Bloch equation may be written in a form such that it is straightforward to obtain the term of equation 2.8 which gives the distant collisions contribution. For such purpose, the ω_0 parameter has to be inserted in the logarithm term inside the bracket of equation 2.7 and, in consequence, a $\frac{1}{2}$ factor accompanying this term should be introduced.

$$-\left(\frac{dE}{d\xi}\right)_{\omega<\omega_0} \equiv REL_{\omega_0} = \frac{4\pi N_A e^4}{m_e c^2}\frac{Z_{eff}^2}{\beta^2}\frac{Z_2}{A}\left\{\frac{1}{2}\ln\left(\frac{2m_e c^2}{I_0^2}\frac{\beta^2}{1-\beta^2}\omega_0\right) - \frac{1}{2}\beta^2 - S - D\right\}\cdot F \tag{2.9}$$

and, consequently, the other term that gives the close collisions contribution to the corrected Bethe-Bloch formula is

$$\begin{aligned}\left(\frac{dE}{d\xi}\right)_{\omega>\omega_0} &= \frac{4\pi N_A e^4}{m_e c^2}\frac{Z_{eff}^2}{\beta^2}\frac{Z_2}{A}\left\{\frac{1}{2}\ln\left(\frac{2m_e c^2}{\omega_0}\frac{\beta^2}{1-\beta^2}\right)\right. \\ &\qquad \left. -\frac{1}{2}\beta^2 + B + M + C_R - \Delta_R + \Delta_{NS}\right\}\cdot F\end{aligned} \tag{2.10}$$

Equation 2.9 is, by definition, the restricted energy loss REL_{ω_0} of the considered charged particle in the given absorber. Due to the difficulties of calculating theoretically ω_0, its value for an specific absorber is in practice obtained from the best fit to experimental data. It must be stated here that the $\frac{1}{2}$ factor which appears in the β^2 term, are due to the fact that one half of such term (see equation 2.7) is originated by the contribution of close collisions, whereas the other half originates from distant collisions contributions.

In former works done in our group as well as in chapter 1, the REL track formation model based on the corrected Bethe-Bloch equation has been applied in order to identify the charge of ultra heavy ions belonging to the primary cosmic radiation which have been recorded in SSNTD's near the Earth surface [Dom95], [Dom96].

In order to evidence the energy dependence of REL_{ω_0}, this magnitude has been plotted versus the energy per nucleon (ε) in figure 2.1 for a given charge. Restricted energy loss (in MeV·cm^2/g units) has been calculated by means of equation 2.9 for energies ranging

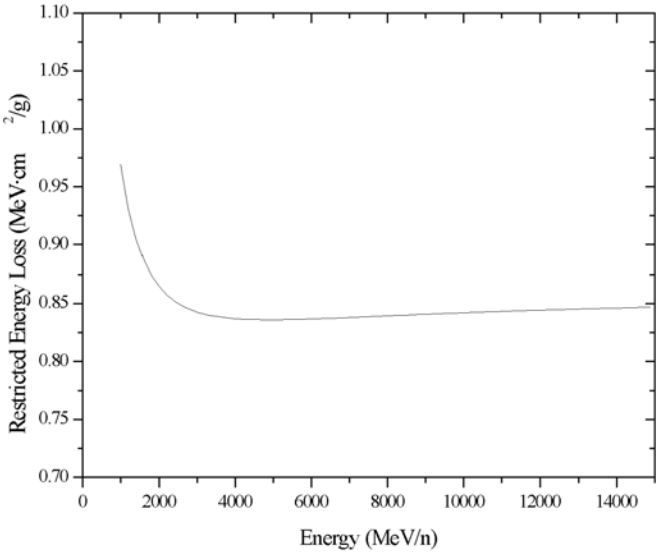

Figure 2.1. REL as a function of the incident ion energy for $Z = 78$. The calculation of REL is based on the corrected Bethe-Bloch formula given in equation 2.9.

from 10^3MeV/n up to $1.5{\cdot}10^3$MeV/n. As figure 2.1 shows, $REL_{\omega0}$remains almost constant for energies above $\approx 3 \cdot 10^3$ MeV/n. The behaviour for other ion charges is similar to that illustrated in figure 2.1.

2.2.3. The Identification method

Charge identification is based on the relationship between the signal recorded in the detector, characterized by the reduced etch rate (S), and REL_{ω_0} which has a potential form

$$S = g\,(REL_{\omega_0})^h \tag{2.11}$$

where g and h are parameters which must be determined through calibration of the detector. Equation 2.11 is the most appropriate function fitting the reduced etch rate with the restricted energy loss among other proposed empirical functions which depend on the detector used, the kind of recorded particles and the energy range in which the identification is carried on [Seq76], [Fer81], [Lüc82] and [Vid84].

Although the approximation of β constant can be assumed in order to identify the charge of the recorded ions [Dom95]'[Dom96], if it is considered that the ions resulting in the recorded tracks lose a small but measurable amount of energy inside the stack, an identification method based on the fractional gradient of the reduced etch rate (RERFG) may be applied [Fow77a], [Fow77b], as has been described in chapter 1. According to the RERFG method, G is defined as

$$G = \frac{1}{S}\frac{dS}{dx} \tag{2.12}$$

where S is the reduced etch rate and x is the path length. According to this method, each recorded track is characterised by a single (S_{eff}, G_{eff}) couple, which is calculated from the measured set of points (x_i, S_i) using expressions 2.13 and 2.14.

$$S_{eff} = \frac{n}{\sum_{i=1}^{n} \frac{S_i + S_{2n+1-i}}{2S_i S_{2n+1-i}}} \tag{2.13}$$

$$G_{eff} = \left| \frac{\sum_{i=1}^{n} \left[\frac{2(S_{2n+1-i} - S_i)w_i}{(S_{2n+1-i} + S_i)\Delta x_i} \right]}{\sum_{i=1}^{n} w_i} \right| \tag{2.14}$$

A charge value may be assigned to every (S_{eff}, G_{eff}) couple, and hence to every recorded track, by knowing which $S_Z(G)$ curve is the closest to the considered (S_{eff}, G_{eff}) point. The $S_Z(G)$ curve is determined varying the energy in equations 2.11 and 2.12 for each given charge, thus the knowledge of the proper values of the parameters g and h, which characterize the detector response, is needed in order to identify the charge and energy of a recorded ion.

On an ideal case, the parameters value should be obtained from calibration in accelerator. In particular, for the SSNTD's used in the *Ultra Heavy Cosmic Ray Experiment* (UHCRE), which was able to detect nuclei with $Z > 65$ and energies above 3 GeV/n, our group performed some calibration work at the Berkeley Bevalac accelerator with ion beams of an energy $\lesssim$ 1GeV/n. Consequently, g and h should be corrected to extrapolate the detector response above $\gtrsim$ 3 GeV/n. A second calibration is required in order to determine the correct value of g and h parameters, this calibration has been performed from the knowledge of the most prominent ion peaks belonging to the charge region considered corresponding to Platinum ($Z = 78$) and Lead ($Z = 82$) peak (see section 3.3 of chapter 1 for a detailed description) . It is also very important to take into account the dependence on energy of the parameters g and h for a proper charge identification.

It should be emphasised the variation of REL_{ω_0} with the energy of the incident charged particle (depicted in figure 2.1), because it may be responsible for the energy dependence of the parameters g and h. This feature, has suggested that the REL track formation model may not be fully applicable, thus a modification of such model is proposed in order to avoid this "local" behavior of the g and h parameters. In the modified REL model a contribution of the close collisions to the amount of energy loss responsible of the latent track formation is taken into account. The close collisions contribution could be relevant but should be small instead of strictly zero as considered in the REL model.

2.3. The modified Restricted Energy Loss track formation model

According to the REL track formation model only distant collisions contribute to the process of latent track formation. This fact is mathematically reflected in equation 2.9, which is the analytical expression of the fraction of stopping power contributing to track formation if the corrected Bethe-Bloch formula is employed. Probably all corrections described above (see table 2.1) would influence the fraction of stopping power contributing to track formation, and therefore to the analytical expression of REL. One should quantify which part of these corrections contribute to track formation or, in other words, find out, if possible at all, which part of the corrections is due to distant collisions and which one is due to close collisions. It must be emphasised that close and distant collisions are extreme approximations of the way in which collisions are treated in the mathematical formalism, so that there is no practical way to separate their contributions, and therefore in most cases it is impossible to distinguish their influence in the analytical expressions of the corrections. One possibility of dealing with this problem might be to introduce a new parameter to be determined semiempirically in the track formation model, taking into account which fraction of the close collision correction terms in the corrected Bethe-Bloch formula (2.7) contribute to the formation of the latent track and consequently to the modification of the REL expression (2.9). This "modified" model of track formation should lead, ideally, to a relationship between signal strength or detector response and the quantity REL not depending on the charge and energy of the incident particle or, in other words, to "universal" values of the g and h parameters which appear in this relationship.

2.3.1. The contribution of close collisions

At this point, one should find out which, if any, of the terms added for correcting the energy loss expression contribute to track formation. This may not be an easy job, since although it seems clear that only those terms related to distant collision contributions are relevant, one must remember that the separation between close and distant collisions is somehow artificial and there is not a clear boundary among them. On the other hand, some terms may display contributions from both kinds of collisions, which might not be possible to separate.

As a first approximation, the Bloch and relativistic Bloch corrections, together with the Mott, the Leung and the Nuclear Size corrections are due to close collision contributions, so they should not contribute to REL and, therefore, to track formation. The density correction, due to distant collisions, and the inner shell correction and the low velocity correction, due to both close and distant collisions, may contribute to some extent to REL. In any case, the contribution of the inner shell correction and that of the Leung correction are not considered in our work because it can be shown that, for swift heavy ions losing energy in an absorber such as plastic track detectors, it is negligible except,

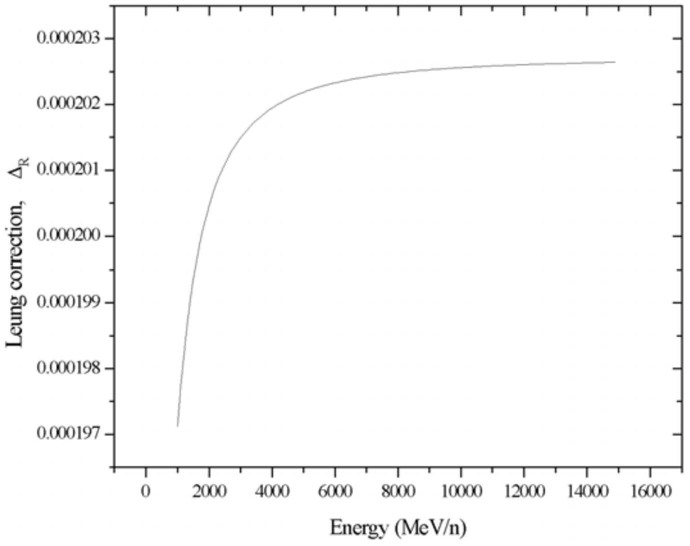

Figure 2.2. The Leung correction as a function of energy for a Pb ion ($Z = 82$) penetrating a plastic detector.

may be, in a very small region of the track of the incident ion, when it almost completely stops, as the velocity of the ion is comparable to that of the atomic electrons. Figure 2.2 shows the very small contribution of the Leung term for energies from 1 GeV/n up to 15 GeV/n corresponding to a Pb ion traversing a SSNTD. On the other hand, the low velocity correction is not taken into consideration as we have made the approach of dealing with the effective charge of the incident ion, which accounts for the same physical process. Finally, it is assumed that energy deposition by bremmstrahlung does not contribute to track formation, thus the ultrarelativistic correction is not included.

It does not seem realistic to consider that the contribution to REL of the processes involving close collisions is exactly zero. If it were so, that would mean that no energy deposited by the recoil electrons, which are expelled far away from the incident particle path, is left in the track neighbourhood, thus implying that this expelled electron has somehow "jumped away" over this neighbourhood and has started to deposit energy once far apart from the track. To take this circumstance into consideration, it is assumed that all distant collision processes contribute fully to track formation and, therefore, to REL. It is also considered that the relevant close collision terms (*i.e.* the Mott, Bloch, relativistic Bloch and nuclear size corrections) may contribute partially to REL. A modified REL track formation model (hereinafter MREL) is proposed in which close and distant collisions contribute to the latent track formation. In order to quantify the partial contribution of

Table 2.2. Values of the factor $\gamma A^{1/3}$ for three different isotopes belonging to the UHCRE's charge region, with two different energy values also characteristic to nuclei recorded in UHCRE.

	Pt^{78}_{195}	Pb^{82}_{208}	U^{92}_{238}
3 GeV/n	24.5	25.0	26.2
5 GeV/n	36.9	37.7	39.5

close collisions a parameter (κ), ranging from 0 to 1, which multiplies the contribution of all close collision terms to the MREL, is defined. The expression of MREL giving the fraction of the energy deposited in the detector by the penetrating particle that contributes to the track formation, is written as:

$$MREL_{\kappa} \equiv -\left(\frac{dE}{d\xi}\right)_{\omega<\omega_0} - \kappa \cdot \left(\frac{dE}{d\xi}\right)_{\omega>\omega_0} \tag{2.15}$$

where the first term $\left(\frac{dE}{d\xi}\right)_{\omega<\omega_0}$, which accounts for the distant collisions contribution, is actually REL_{ω_0} defined in equation 2.9.

In order to obtain an expression which allows to calculate the $MREL_{\kappa}$ quantity, .equation 2.15 can be developed using equations 2.9 and 2.10,

$$\begin{aligned} MREL_{\kappa} &= \frac{4\pi N_A e^4}{m_e c^2}\frac{Z_{eff}^2}{\beta^2}\frac{Z_2}{A}\left\{\left[\frac{1}{2}\ln\left(2m_e c^2\frac{\beta^2}{1-\beta^2}\right)-\frac{\beta^2}{2}\right](1+\kappa)\right. \qquad (2.16) \\ &\left. + \frac{1}{2}(1-\kappa)\ln(\omega_0) - \ln(I_0) + (B+M+C_R)\,\kappa\right\} \end{aligned}$$

For the limit value of $\kappa = 0$ the classic REL expression (equation 2.9) is recovered, whereas for the opposite value $\kappa = 1$, equation 2.16 equals the corrected Bethe-Bloch formula (equation 2.7).

When ultra heavy nuclei with charge and energy similar to those detected in the UHCRE experience (*i.e.* $Z \gtrsim 65$ and $\varepsilon \simeq 3-5$ GeV/n) are considered, the nuclear size correction, Δ_{NS}, can be removed from equation 2.16 as its validity condition $\gamma A^{1/3} \approxeq 160$ [Dat96] is not achieved for such particles (see table 2.2 with the values of $\gamma A^{1/3}$ factor for three different isotopes of the UHCRE's charge region and energies of 3 GeV/n and 5 GeV/n).

The Bloch correction, B, has been evaluated using the series [Abr72]:

$$B \equiv \psi(1) - \mathrm{Re}\,\psi(1+iv) = -v^2\sum_{n=1}^{\infty} n^{-1}\left(n^2+v^2\right)^{-1} \tag{2.17}$$

The expressions employed to calculate the density effect, D, are given in [Ste82], [Ste71] and [Ste81] which are obtained from a semiempirical fit to experimental data. The

Mott correction, M, is calculated by means of the expression given in [Ahl78], [Ahl80], which fails at low energies of the incident particle as it does not vanish when $\beta \to 0$. In order to overcome this failure, the correction has been assumed to be constant and equal to its estimated uncertainty given by $(Z_{eff}\alpha)^9 / 6\beta^9$, when the correction achieve values very similar to the uncertainty ones, following the criteria given in [Wad83]. The relativistic Bloch correction, C_R, calculation is performed using the expressions provided by [Ahl82]. For this calculation, the semiempirical fit of two parameters is required; the dispersion angle θ_0 which allows to separate the close collisions into those where the transverse momentum is negligible and those where it is not, and the impact parameter, λ, which allows to distinguish between close and distant collisions. The values of the relativistic Bloch correction does not depend strongly on the λ value, nevertheless it is quite sensitive to the value of θ_0. The values of $\theta_0 = 0.1$ and $\lambda = 1$ have been taken as a first approach, as suggested in [Ahl82] when it is assumed that an impact parameter equal to the Bohr radius differentiates the close collisions to the distant ones (see [Mom94] for the expressions of each correction).

In order to evidence the contribution of the close collision corrections to the $MREL_\kappa$, several figures are displayed. In figures 2.3, 2.4 and 2.5 the Bloch correction (B), the Mott correction (M) and the quantic Bloch correction (C_R) for a given nuclei of $Z = 80$ are plotted as a function of energy for several values of the close collision contribution parameter, κ. The behaviour of such curves for other nuclei are similar to that shown in these figures. On the other hand, figures 2.6, 2.7 and 2.8 illustrate the energetic dependence of the Bloch correction (B), the Mott correction (M) and the quantic Bloch correction (C_R) at a fixed value of the parameter $\kappa = 0.2$ for different ions ($Z = 70$, 80 & 90). Curves for other values of the κ parameter offer similar behaviour to that for $\kappa = 0.2$. According to figures 2.6 and 2.8 it is inferred that the higher the considered charge is the much relevant the contributions of both Bloch corrections, B and C_R, to the $MREL_\kappa$ are, contrarily to what happens with the contribution of the Mott correction, M. as shown in figure 2.7.

Figure 2.9 shows, as an example, the $MREL_\kappa$ graphs obtained as a function of the incident ion energy for different κ values and for a given ion charge (in this case, Z = 78). The behaviour for other ion charges is similar. In this figure, one can see clearly that, as expected, $MREL_\kappa$ increases when the close collisions contribution increases. In addition, the minimum of ionisation shifts to lower energies when κ increases, and the gradient of $MREL_\kappa$ for energies above this minimum is more prominent also when κ increases. Taking into consideration that no ion with energy below 3 GeV/n is recorded in the UHCRE, one can see that, if $\kappa = 0.0$, $MREL_\kappa$ remains nearly constant as the incident ion slows down, increasing slightly when its energy is close to 3 GeV/n. As κ increases, one finds that as the incident ion slows down to 3 GeV/n, its $MREL_\kappa$ decreases, so that the recorded signal strength decreases according to equation 2.11. This situation is opposite to that normally assumed for slowing down ions when no close collision corrections to the Bethe-Bloch formula, nor to the modified REL, are taken into account. This analysis puts into

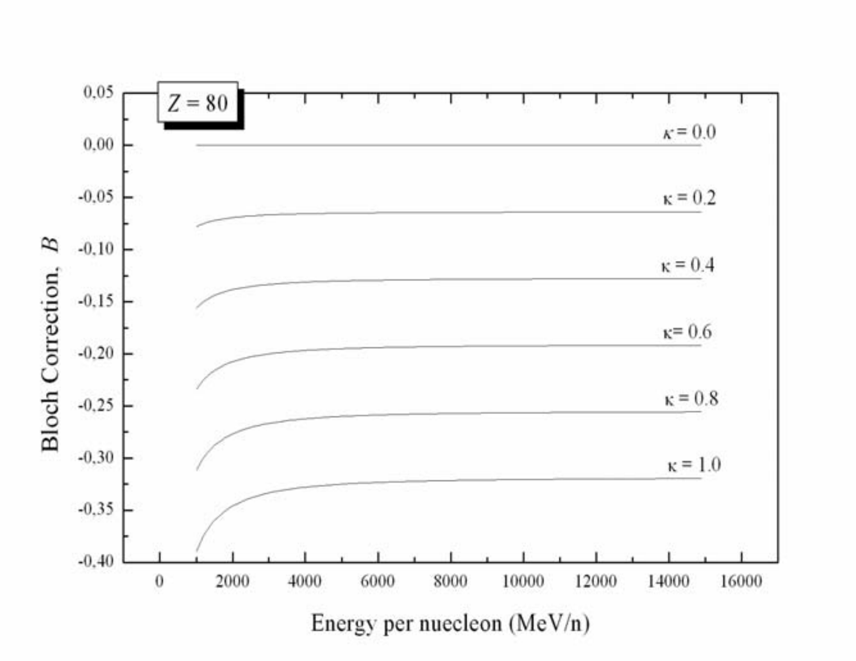

Figure 2.3. The Bloch correction term as a funtion of energy of a $Z = 80$ ion mudulated by several values of the close collisions contribution parameter, κ.

evidence that the knowledge of the restricted energy loss mechanism, and that of the close collisions contribution, is the key for the correct assignment of charge to the incident ion.

2.3.2. Study of the behaviour of the MREL model parameters

In order to evaluate the effect of using the modified restricted energy loss (MREL) track formation model instead of the classic REL one, the MREL model together with the reduced etch rate fractional gradient method (RERFG), as charge identification process, is applied to nuclei recorded in the UHCRE experience. Mathematically speaking, this charge assignation process is translated into determining the $S_Z(G)$ curves from equations 2.11 and 2.12 replacing the REL_{ω_0} term by the new $MREL_\kappa$ term which, in turn, can be calculated with equation 2.16. Therefore, equation 2.11 is updated and may be written as

$$S = g\left(MREL_\kappa\right)^h = g\left[\left(\frac{dE}{d\xi}\right)_{\omega<\omega_0} + \kappa\left(\frac{dE}{d\xi}\right)_{\omega>\omega_0}\right]^h \tag{2.18}$$

According to this equation 2.18, the new parameter introduced in the MREL model, κ, takes part in the determination of the $S_Z(G)$ curves. As this parameter can vary freely in the range from 0 to 1, it does not exist a unique $S_Z(G)$ curve for a fixed ion charge, given the values of the parameters g and h. At this point, an appropriate calibration

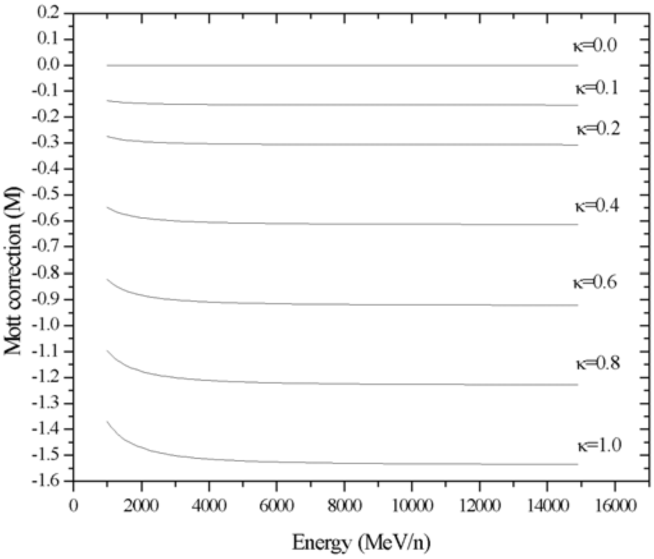

Figure 2.4. The Mott correction term as a funtion of energy of a $Z = 80$ ion mudulated by several values of the close collisions contribution parameter, κ.

should be required in order to determine the correct value of the parameter κ and, hence, to proceed with the identification process as described in section 2.3.

The abundance peaks in the charge region, where the nuclei seen by the plastic detectors of the UHCRE belong, are those corresponding to the Platinum ($Z = 78$) and the Lead ($Z = 82$) dominant elements. In order to evaluate the effect that the close collisions contribution parameter, κ, could have on the parameters of the identification method, a procedure (hereinafter *parameter procedure*) based on the reproduction of the Pt-Pb abundance peaks has been developed and applied. It must be stated that this parameter procedure does not consist on a calibration because the κ parameter is not determined although g and h parameters are for a given fixed κ value.

The first step of this *parameter procedure* consists on fixing a value for the close collisions contribution parameter, κ (in this case the chosen values are $\kappa = 0.0$, 0.1, 0.2, 0.4, 0.6, 0.8 and 1.0). Next, the values of the parameters g and h are randomly generated instead of determining their value by means of a peak calibration in the way that in section 3.3 of chapter 1 has been done. Values of the parameter h are chosen randomly from the interval (2,4) whereas the g parameter takes values randomly from the interval (1,10). A total of 1500 couples of g and h values are generated for each fixed value of κ.

With each set of values of the parameters κ, g and h, the charge identification method based on the RERFG (as described in subsection 2.2.3.) is performed for a set of

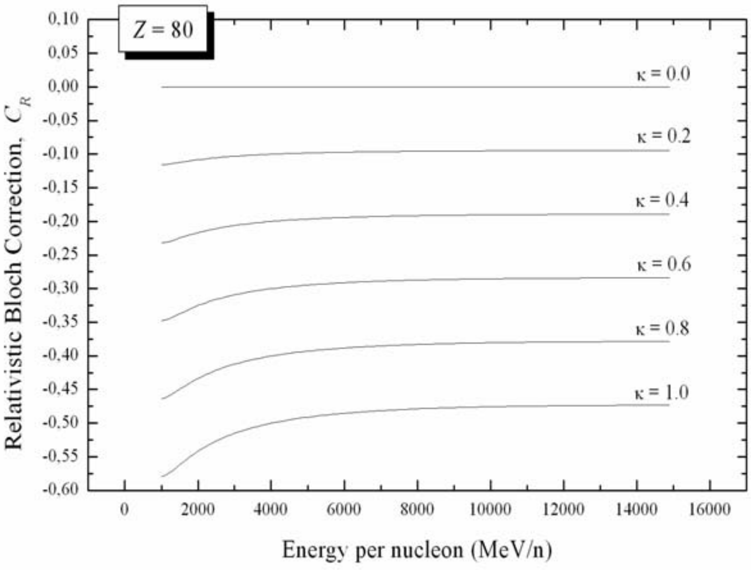

Figure 2.5. The relativistic Bloch correction term as a funtion of energy of a $Z = 80$ ion mudulated by several values of the close collisions contribution parameter, κ.

measurements obtained from the UHCRE, and, hence, a charge histogram is obtained. In order to accept a given set of parameters, two different criteria are applied. The first of such criteria establish that a set of parameters values is correct if the charge histogram obtained from them reproduces the dominant Pt peak in its right position with a tolerance of one charge unit (*i.e.* $Z = 78 \pm 1$). The g and h parameter values filtered under the first criterion are subject to a second criterion which establishes that the selected final values of such parameters are those with which its corresponding charge histogram reproduce, by means of a gaussian fit, the Pt and Pb abundance peak centered at $Z = 78 \pm 1$ and $Z = 82 \pm 1$, respectively. So that, if for a given set of parameters values the two prominent peaks are not located in their right position, that set is refused. In figures 2.10 and 2.11 all couples of g and h parameters are plotted in the $g - h$ plane for two different κ values ($\kappa = 0.0$ and $\kappa = 0.2$). In both figures, selected and refused values according to the second criterion are distinguished.

A surprising feature inferred from both figures 2.10 and 2.11, is that the accepted values of the parameters g and h do not mix with the refused values of such parameters. So that, the set of all selected points in the $g - h$ plane fall into a well defined domain which is not contaminated by the remaining points refused, as can be seen in figures 2.10 and 2.11. The corresponding plots for the rest of κ values also elucidate a domain for the selected values of g and h. The mean value of the g and h values which are contained in a

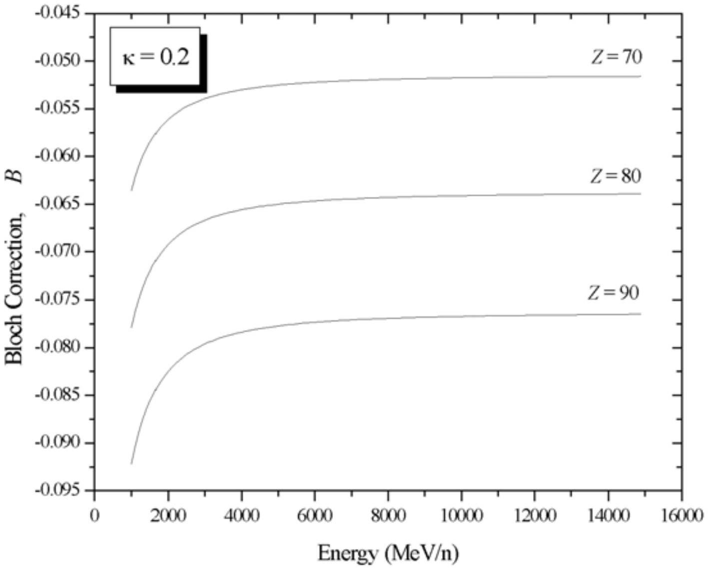

Figure 2.6. The Bloch correction term as a funtion of energy for three diferent ions with $Z = 70$, $Z = 80$ and $Z = 90$, fixing the close collisions contribution parameter $\kappa = 0.2$.

certain domain are calculated in order to characterise such domain. Consequently, for each initially considered value of the close collision contribution parameter, κ, the associated g and h mean value is determined. All this laborious process of parameter selection is synthesised in table 2.3 in which the mean value of g and h parameters obtained for each κ value assumed.

As it can be appreciated from data of table 2.3 , there seems to be a certain correlation between the κ parameter and the mean values of g and h parameters. Two new figures are plotted in order to evidence such correlation. In figure 2.12 the different mean values of the parameter g are plotted versus the corresponding κ value, and in figure 2.13 the h mean values are plotted versus κ. In both figures the best fit to the data is also included. A linear fit is effectuated between κ and g_{mean} parameter values, and regression coefficient of $r^2 = 0.99614$ is obtained. On the other hand, h_{mean} and κ data are better fitted with a parabolic function as confirmed by the calculated regression coefficient ($r^2 = 0.99931$). This result clearly confirms that g and h parameters are not independent of the κ parameter, furthermore, when a larger contribution of the close collisions is considered to take part in the track formation (corresponding to larger values of κ parameter), then, the values of the parameters g and h required to perform a right identification decrease.

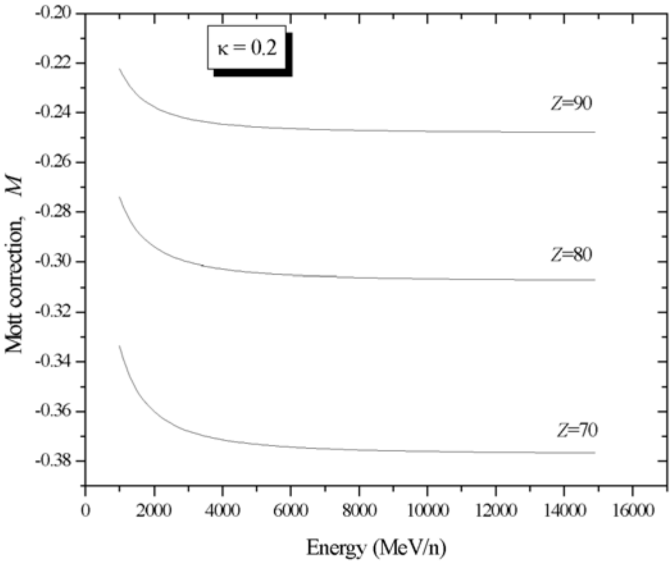

Figure 2.7. The Mott correction term as a funtion of energy for three diferent ions with $Z = 70$, $Z = 80$ and $Z = 90$, fixing the close collisions contribution parameter $\kappa = 0.2$.

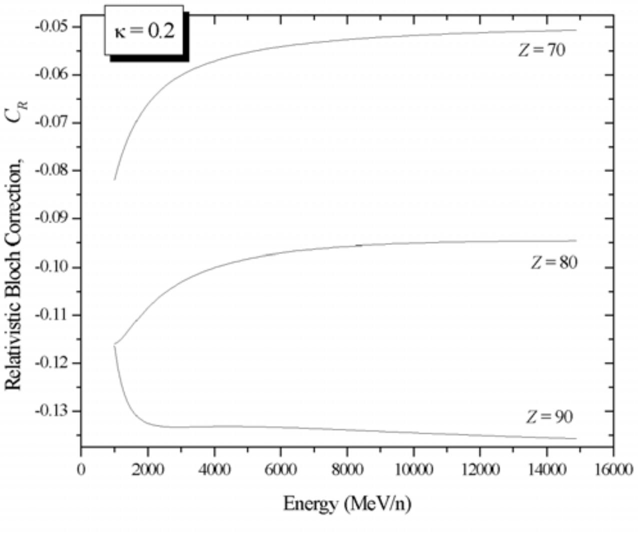

Figure 2.8. The relativistic Bloch correction term as a funtion of energy for three diferent ions with $Z = 70$, $Z = 80$ and $Z = 90$, fixing the close collisions contribution parameter $\kappa = 0.2$.

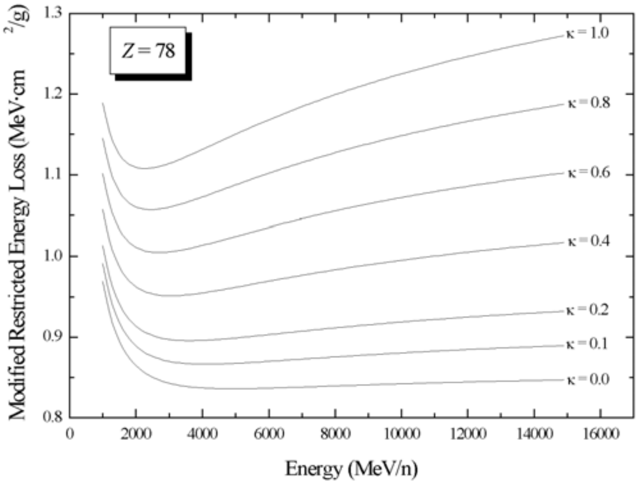

Figure 2.9. The modified REL as a function of the incident ion energy for the indicated values of the close collision contribution parameter κ, and for $Z = 78$. The behaviour for other ion charges is similar. The minimum of ionisation shifts to lower energies when κ increases.

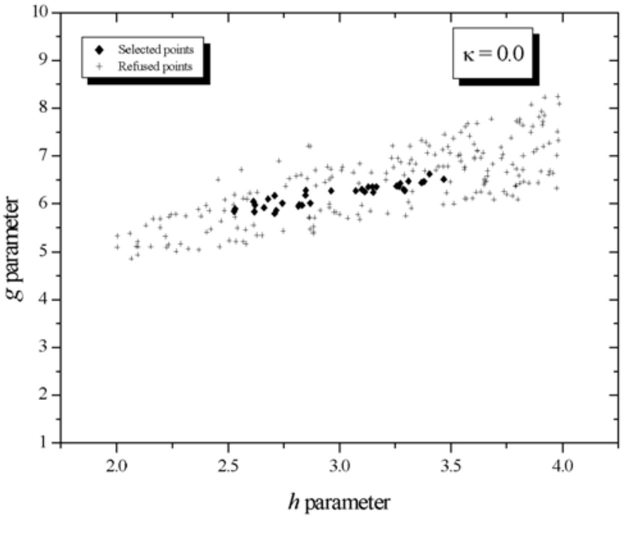

Figure 2.10. Values of the parameters g & h randomly generated for a fixed $\kappa = 0.0$ in the g-h plane. (+) are the points that reproduce only the Pt dominant peak. (♦) are those that reproduce both Pt and Pb peaks.

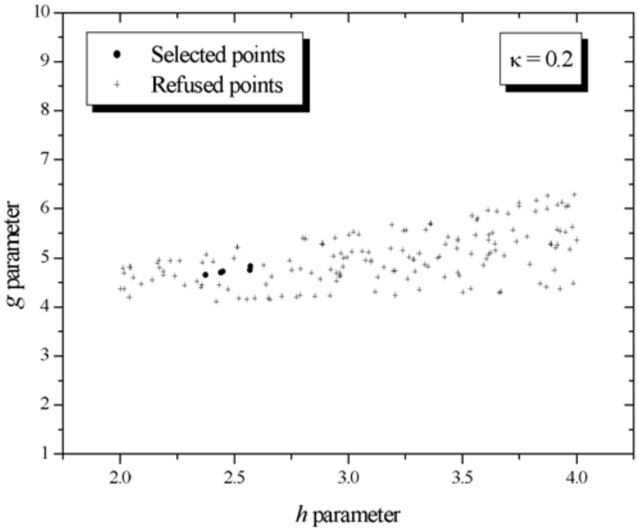

Figure 2.11. Values of the parameters g & h randomly generated for a fixed $\kappa = 0.2$ in the g-h plane. (+) are the points that reproduce only the Pt dominant peak. (♦) are those that reproduce both Pt and Pb peaks.

Table 2.3. The mean values of the g and h parameters corresponding to an assumed k value.

κ value	g mean value	h mean value
0.0	5.79	2.44
0.1	5.11	2.43
0.2	4.84	2.41
0.4	4.09	2.34
0.6	3.48	2.27
0.8	2.77	2.18
1.0	2.19	2.10

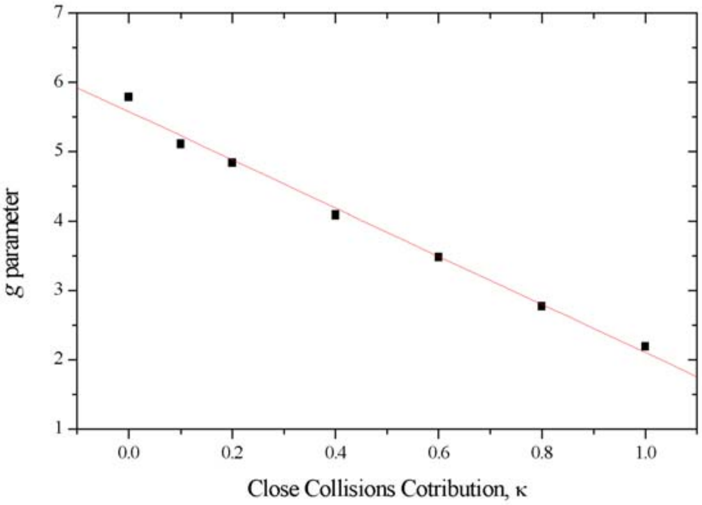

Figure 2.12. g mean values plotted versus κ values. The data are very well fitted by a linear function, which is also included in the figure, with a regresion coeficient value of 0.99614.

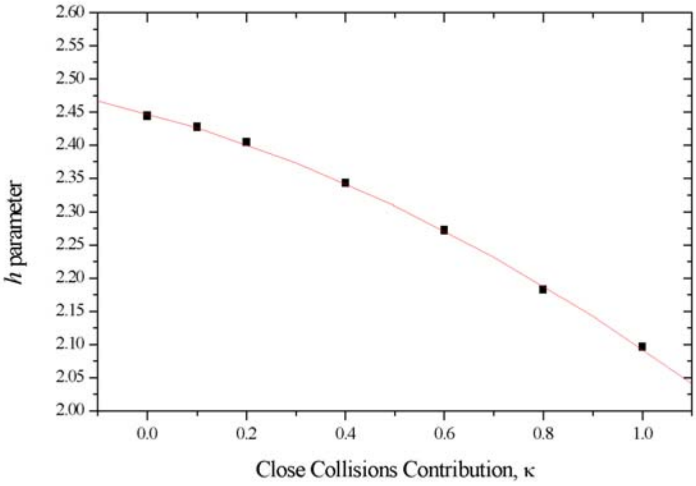

Figure 2.13. h mean values plotted versus κ values. The data are very well fitted by a parabolic function, which is also included in the figure, with a regresion coeficient value of 0.99931.

Table 2.4. Position and full width at half height of the gaissian peaks fitted to the charge histogram for the 205 ultra heavy events recorded in UHCRE for the values of κ indicated.

	κ value	0.0	0.1	0.2	0.4	0.6	0.8
Peak 1	Centre	77.54	78.49	77.49	78.48	76.12	76.14
	Width	5.33	5.88	5.57	6.65	6.68	6.48
Peak 2	Centre	82.6	83.62	83.21	84.63	83.12	83.19
	Width	1.18	1.46	1.23	0.84	1.52	1.72

2.4. Estimation of the Close Collision Contribution parameter of the Modified REL model

As discussed in previous section, the "calibration" procedure applied has not yield a final unique value for the close collision contribution parameter, so that this parameter remains undetermined, although a certain dependence on it has been found for the other two parameters involved on the identification method used in this work. In order to study the range of applicability of the proposed MREL model as a function of the κ parameter, the 205 Ultra Heavy Cosmic Rays recorded in the UHCRE can be used as well as the Bevalac accelerator exposure results.

2.4.1. Estimation with the UHCRE results

In order to check the validity of each set of parameters values (κ, g and h) appearing in table 2.3, the charge identification process based of the RERFG method (as described in section 2.2.3.) is performed again taking the measurements results for the 205 ultra heavy events recorded in the UHCRE experience. The charge histogram obtained for each different set of parameter values are illustrated in figures 2.14, 2.15, 2.16, 2.17, 2.18 and 2.19 in which the two gaussian peaks used to fit the data, as well as its convolution curve, are also plotted evidencing the existence of two abundance peaks which should correspond to the Pb and Pt peaks. Table 2.4 shows the position and the full width at half height of the gaussian peaks fitted.

Comparing the position of the peaks fitted by gaussian peaks in the different histograms with the predicted abundances peaks in this charge region, it might be assessed that the contribution of the close collisions, if existing, should be small. In fact, for those values of κ equal to or larger than 0.4 the overall aspect of the charge spectrum, in particular, the position and the width of both peaks, seems not to be realistic. Thus, this result establishes a limit value for the close collision contribution parameter.

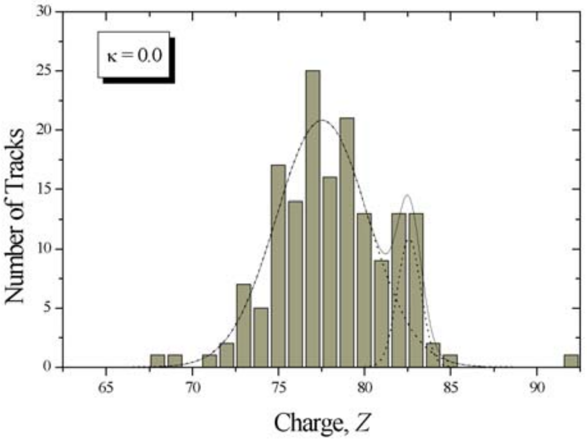

Figure 2.14. Charge histogram obtained for the 205 UHCRE events, when the value of $\kappa = 0.0$ is considered to perform the "calibration" procedure. Best fit with two gaussian peaks and its convolution are plotted.

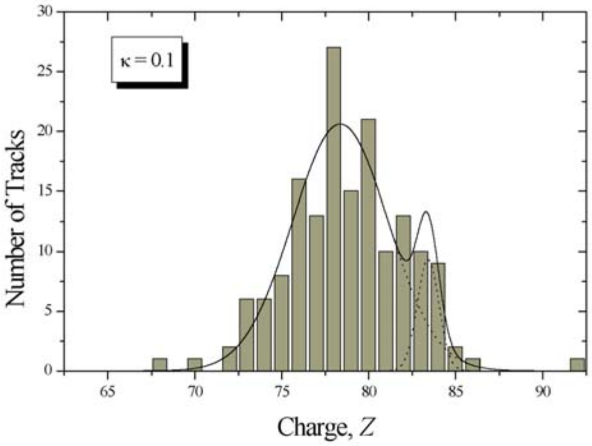

Figure 2.15. Charge histogram obtained for the 205 UHCRE events, when the value of $\kappa = 0.1$ is considered to perform the "calibration" procedure. Best fit with two gaussian peaks and its convolution are plotted.

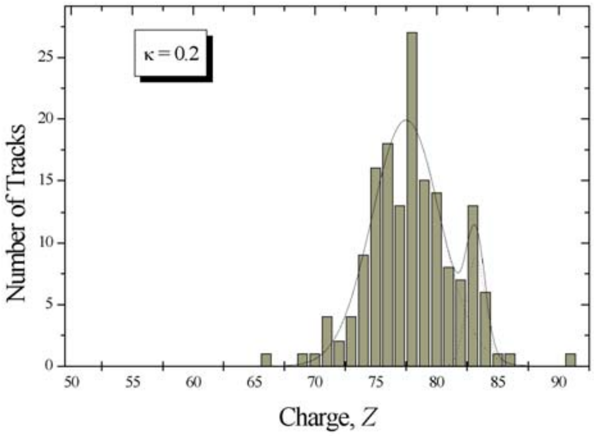

Figure 2.16. Charge histogram obtained for the 205 UHCRE events, when the value of $\kappa = 0.2$ is considered to perform the "calibration" procedure. Best fit with two gaussian peaks and its convolution are plotted.

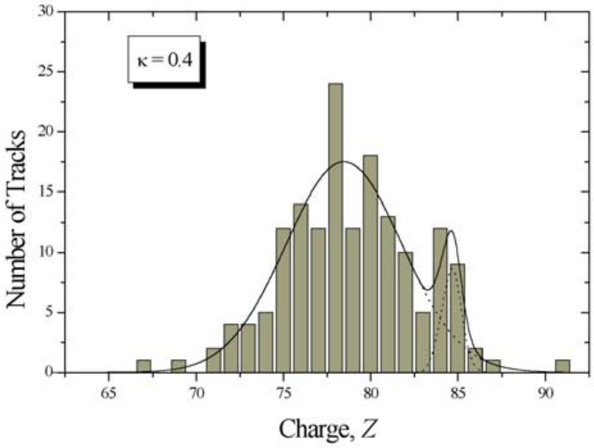

Figure 2.17. Charge histogram obtained for the 205 UHCRE events, when the value of $\kappa = 0.4$ is considered to perform the "calibration" procedure. Best fit with two gaussian peaks and its convolution are plotted.

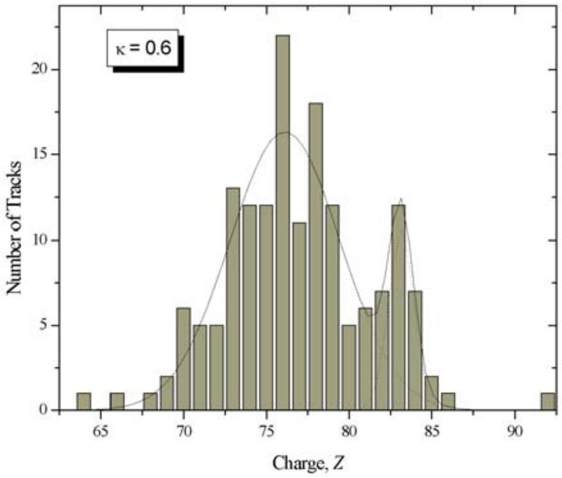

Figure 2.18. Charge histogram obtained for the 205 UHCRE events, when the value of $\kappa = 0.6$ is considered to perform the "calibration" procedure. Best fit with two gaussian peaks and its convolution are plotted.

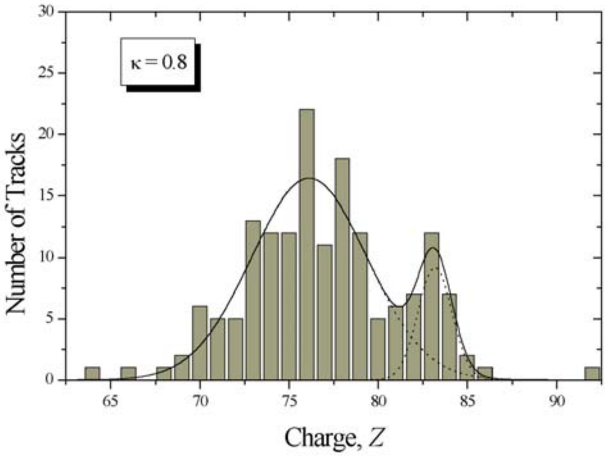

Figure 2.19. Charge histogram obtained for the 205 UHCRE events, when the value of $\kappa = 0.8$ is considered to perform the "calibration" procedure. Best fit with two gaussian peaks and its convolution are plotted.

2.4.2. Estimation with the accelerator data

Several stacks of plastic detectors have been exposed to relativistic ultra heavy ions at the heavy ion accelerator in Berkeley, Bevalac. A part of these stacks were used to study the response of SSNTD of different kind to relativistic ultra heavy ions as well as the environmental effects that could alter this response. The remaining stacks, which were mounted on board of the *Long Duration Exposure Facility* (LDEF) satellite as a part of the UHCRE experience, were exposed in the Bevalac accelerator before the LDEF was launched to the Earth orbit and after its retrieval in order to study the stability of the detector response and also to perform the calibration of them. The analysis of all these stacks has been carried on by our group at the Universitat Autònoma de Barcelona.

In this work, only the stack named as LP, which is build by plates of Lexan polycarbonate, is employed to perform the MREL track formation model. The LP stack were exposed to Uranium ions with an initial kinetic energy of 919 MeV/n and to Gold ions with an energy of 990 MeV/n. A total of 8 tracks originated by the U ions, and 8 tracks corresponding to the Au incident ions have been located and measured.

In order to perform our calibration, an (S_{eff}, G_{eff}) point, which characterises the considered track, is calculated using equations 2.13 and 2.14 for each measured track. On the other hand, taking different values of the close collisions contribution parameter, κ, a set of $S_Z(G)$ curves for a given charge, are generated using equations 2.18 and 2.12. In our case, a total of 8 curves corresponding to the values of $\kappa = 0.0$, 0.1, 0.2, 0.4, 0.5, 0.6, 0.8, and 1.0 are obtained for each fixed charge value of $Z = 79$ (Au) and $Z = 92$ (U). Figure 2.20 and figure 2.21 show the set of $S_Z(G)$ curves corresponding to Au ions and U ions, respectively, the (S_{eff}, G_{eff}) points for each measured track are also plotted. The mean value of (S_{eff}, G_{eff}) and its standard deviation taken as error bar which characterises the cloud of experimental points are also included in both figures.

The estimated value of the κ parameter provided by the calibration process is obtained from knowing which $S_Z(G)$ curve contains the (S_{eff}, G_{eff}) mean value, as each of such curves is labelled by its corresponding κ value. In the case that the (S_{eff}, G_{eff}) mean value would not be contained in any of the plotted curves, a linear interpolation is performed, and taking into account the error bars an estimated uncertainty of κ is determined. An estimated value of $\kappa = 0.26 \pm 0.06$ is obtained from the calibration with Au ions (see figure 2.20), whereas a value of $\kappa = 0.36 \pm 0.06$ is obtained from the calibration with U ions (see figure 2.21). These two results are compatible if the associated uncertainties are taken into account. In addition, these values are both in agreement with the limit value of $\kappa = 0.4$ found in the previous subsection 2.4.1..

2.5. Discussion and conclusions

In this chapter, a modified track formation model based on the known REL one has been proposed with the aim to improve the identification process of ultra heavy ions

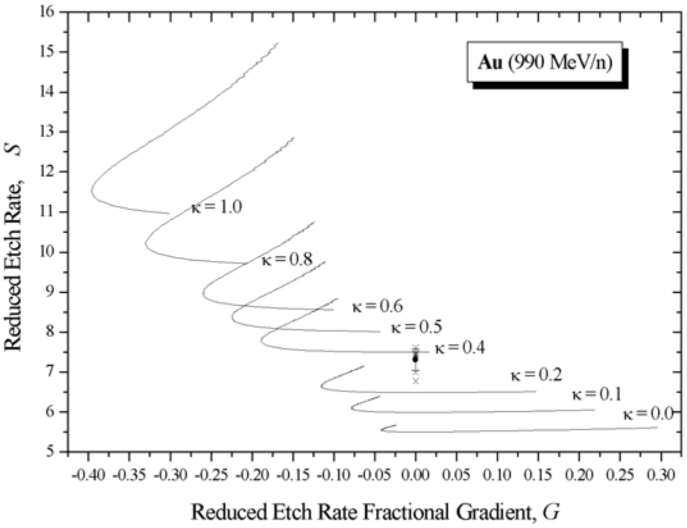

Figure 2.20. Several $S_Z(G)$ curves for Gold ($Z = 79$) obtained for different values of the κ parameter. Experimental (S_{eff}, G_{eff}) points calculated from accelerator results are also plotted.

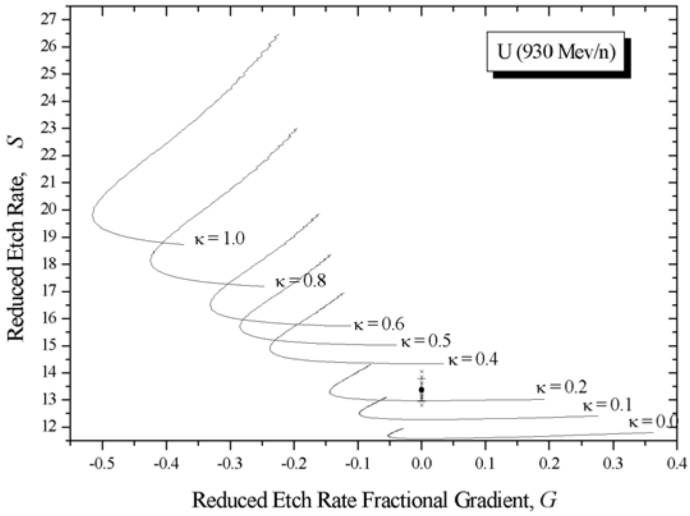

Figure 2.21. Several $S_Z(G)$ curves for Uranium ($Z = 92$) obtained for different values of the κ parameter. Experimental (S_{eff}, G_{eff}) points calculated from accelerator results are also plotted.

as those arriving at the Earth atmosphere belonging to primary cosmic radiation which are detected using solid state nuclear tracks detectors. The motivation for the modified restricted energy loss model is found from several features arisen when the REL model is applied:

> *i*) The identification process is supported by the determination of the values of the g and h parameters by means of an adequate calibration. It has been found that both parameters are energy dependent, and hence, the identification process based on the RERFG method reveals a "local" behaviour.
>
> *ii*) The REL model only takes the contribution of the distant collisions to the formation of the latent track, consequently, the REL_{ω_0} quantity do not shows any variation for an energy above ~ 3 GeV/n and for any given charge.
>
> *iii*) The terms in the corrected Bethe-Bloch equation, which respond to the contribution of the close collisions such as the Bloch correction, the Mott correction and the quantic Bloch correction, exhibit a dependence with the energy.
>
> *iv*) Close and distant collisions are extreme approximations of the way in which collisions are treated in the mathematical formalism, actually, the ω_0 parameter takes care of distinguishing between both collisions, so that there is no practical way to separate their contributions.

If the close collisions are considered to take part to the latent track formation process, the price that has to be paid is the introduction of a new parameter accounting for which fraction of these collisions contribution is involved to the track formation. With this parameter, κ, the track formation model acquires a more physical significance as it seems to be more realistic that close collisions (actually, a fraction of them) also contribute together with distant collisions to the process of latent track formation. In order to study the MREL model, data from the Bevalac accelerator exposures to relativistic heavy ions are used as well as results of the recorded ions in the UHCRE experience.

In this second case, a *parameter procedure* is performed which consists on randomly generate values of g and h for a fixed κ value, and only select those values that properly reproduce the Pt and Pb peak. The agreement between the mean value of $g = 5.79$ and $h = 2.44$ corresponding to $\kappa = 0.0$ and those obtained in chapter 1 by means of a real peak calibration when the REL track formation model is applied ($g = 5.899$, $h = 2.466$), may confirm the validity of the "calibration" procedure used in this work.

A dependence of g and h on κ has been found as illustrated in figures 2.12 and 2.13 which can be respectively very well fitted by a linear and a parabolic function. The most relevant feature is that these fitting functions are both decreasing functions. Thus, when a higher contribution to the track formation of the close collisions is assumed (increasing the κ value), the model, somehow responds decreasing the values of g and h as if some kind of equilibrium would be required to achieve. This behaviour seems to suggest that it doesn't matter where the contribution to the energy loss, which is responsible to the track formation, comes from, nevertheless a fraction of the total energy loss (without distinguishing between close and distant collisions) would be the relevant magnitude to latent track formation. Mathematically this could be written as

$$S = \eta \left(\frac{dE}{dx} \right) \tag{2.19}$$

being S the reduced etch rate, $\left(\frac{dE}{dx}\right)$ the stopping power which can be calculated using the corrected Bethe-Bloch formula given in equation 2.7, and η the unique parameter of the model which could be determined by means of a simple calibration based on dominant abundance peak or on accelerator relativistic ions exposures, instead of the three parameters (κ, g, h) required in the MREL model. The η parameter dependence on the charge and energy is needed in order to properly perform the charge assignation procedure in which, equation 2.19 plays the same role as equation 2.11 or 2.18 in the case of using the REL or the MREL track formation model, respectively. In order to find, if it exists, these dependences of the parameter η, calibration to ions with different charge and energy would be required.

The study of the MREL model realized with exposures to Au and U ions in the Bevalac accelerator has provided a value of $\kappa = 0.26 \pm 0.06$ and $\kappa = 0.36 \pm 0.06$, respectively. Both results are in agreement with the limit value of $\kappa \lesssim 0.4$ obtained by means of the application of this model to the UHCRE results. So, it has been possible to determine values for κ parameter with which the ultra heavy cosmic rays recorded in UHCRE with an energy over ~ 3 GeV/n are identified correctly, as well as the Au and U ions from accelerator with an energy of ~ 1 GeV/n. A certain dependence of the κ parameter with the charge considered may be concluded due to the difference between the values of this parameter when the study is performed taken the Au ions ($Z = 79$) or the U ions ($Z = 92$). As the energies of the Bevalac accelerator ions with which we have worked on are very similar (919 MeV/n for U and 990 MeV/n for Au), an energy dependence of this parameter cannot be concluded. Thus, new exposures to Au or U ions at different energies to those involved in this work would be required in order to confirm this dependence with the energy.

In order to improve charge assignment, one possibility for future work is to consider individually the contribution of each of the close collision terms to the MREL and, hence to track formation. In consequence, the close collision contribution parameter κ is splitted into several new parameters, κ_i, each of them accounting for the fraction of the considered close collision term which takes part in the track formation process. The introduction of such parameters could allow to remove any energy dependence of them and consequently, the identification method would acquire an "universal" behaviour.

References

[Abr72] M. Abramowiwitz & I.A. Stegun, Handbook of mathematical functions (Dover, New York, 1972) 258.

[Ada86] J.H. Adams & L.P. Beahm, Nucl. Tracks and Radiat. Meas. **12** (1986) 387.

[Ahl78] S. P. Ahlen, Phys Rev. A **17** (1978) 1236.

[Ahl80] S. P. Ahlen, Rev. Mod. Phys. **52** (1980) 121.

[Ahl82] S. P. Ahlen, Phys Rev. A **25** (1982) 1856.

[Bar63] W.H. Barkas, Nuclear research emulsions (Academic Press, New York, 1963).

[Ben68] E.V. Benton & R.P. Henke, Nucl. Instr. and Meth. **58** (1968) 241.

[Ben69] E.V. Benton & W.D. Nix, Nucl. Instr. and Meth. **67** (1969) 343.

[Bet30] H. Bethe, Ann. Phys. **5** (1930) 325.

[Bet32] H. Bethe, Z. Phys. **76** (1932) 293.

[Bic92] H. Bichsel, Phys Rev. A **46** (1992) 5761.

[Bim92] R. Bimbot, Nucl. Instr. and Meth. B **69** (1992) 1.

[Blo33] F. Bloch, Ann. Phys. **16** (1933) 285.

[Boh13] N. Bohr, Philos. Mag. **25** (1913) 10.

[Boh15] N.Bohr, Philos. Mag. **30** (1915) 581.

[Boh48] N. Bohr, K. Dan. Vidensk. Selsk. Mat.-Fys. Medd. **18** (1948) 18.

[Dat96] S. Datz et al., Phys. Rev. Lett. **77** (1996) 2925.

[Dom87a] C. Domingo *et al.*, Proc. 20th International Cosmic Ray Conf. (Moscow, 1987) vol. **2** p. 406.

[Dom87b] C. Domingo *et al.*, Nucl. Tracks Radiat. Meas. **15** (1987) 47.

[Dom90] C. Domingo *et al.*, Proc. 21st Int. Cosmic Ray Conf. (Adelaide, 1990) vol. **4** p. 437.

[Dom95] C. Domingo *et al.*, Proc. 24th International Cosmic Ray Conf. (Rome, 1995) vol. **2** p. 572.

[Dom96] C. Domingo *et al.*, Rad. Meas. **26** (1996) 825.

[Dra87] J. Drach, Ph. D. Thesis (University of California, Berkeley, 1987).

[Fan63] U. Fano, Annu. Rev. Nucl. Sci. **13** (1963) 1.

[Fer81] F. Fernández *et al.*, Proc.11th Int. Conf. SSNTD (Bristol, 1981) 261.

[Fle64] R.L. Fleischer *et al.*, Phys. Rev. **133** (1964) 1443.

[Fle65] R.L. Fleischer *et al.*, J. Appl. Phys. **36** (1965) 3645.

[Fle67] R.L. Fleischer *et al.*, Science **155** (1967) 187.

[Fow77a] P.H. Fowler *et al.*, Proc. 9th Int. Conf. SSNTD (Munchen, 1977) 1007.

[Fow77b] P.H. Fowler *et al.*, Nucl. Instr. and Meth. **147** (1977) 195.

[Gei82] H. Geissel et al., Nucl. Instr. and Meth. **194** (1982) 21.

[Her91] J. Herault *et al.*, Nucl. Instr. and Meth. B **61** (1991) 156.

[Leu89] P.T. Leung, Phys Rev. A **40** (1989) 5417.

[Lin96] J. Lindhard & A.H. Sørensen, Phys Rev. A **53** (1996) 2443.

[Lüc82] H.B. Lück, Nucl. Instr. and Meth.in Phys. Res. **198** (1982) 611.

[Mom94] J. Mompart, Master in Science Thesis (Universitat Autònoma de Barcelona), 1994).

[Nor63] L.C. Northcliffe, Annu. Rev. Nucl. Sci. **13** (1963) 67.

[Osu87] D. O'Sullivan *et al.*, Proc. 20th International Cosmic Ray Conf. (Moscow, 1987) vol. 2 p. 410.

[Pie68] T.E. Pierce & M. Blann, Phys Rev **173** (1968) 390.

[Pri86] P.B. Price & M.H. Salamon, Nucl. Tracks and Radiat. Meas. **12** (1986) 5.

[Pri87] P.B. Price & J. Drach, Nucl. Instr. and Meth. **B 28** (1987) 275.

[Seq76] J. Sequeiros *et al.*, Nucl. Instr. and Meth. **135** (1976) 133.

[Ste71] R.M. Sternheimer & R.F. Peierls, Phys Rev. B **3** (1971) 3681.

[Ste81] R.M. Sternheimer, Phys Rev. B **24** (1981) 6288.

[Ste82] R.M. Sternheimer et al., Phys Rev. B **26** (1982) 6067.

[Tho86] A. Thompson *et al.*, Nucl. Tracks and Radiat. Meas. **12** (1986) 391.

[Tho87] A. Thompson *et al.*, Proc. 20th International Cosmic Ray Conf. (Moscow, 1987) vol. 2 p. 401.

[Wad83] C.J. Waddington et al., Phys Rev. A **28** (1983) 464.

[Wad86] C.J. Waddington *et al.*, Phys. Rev. A **34** (1986) 3700.

[Vid84] A. Vidal-Quadras *et al.*, Nucl. Instr. and Meth.in Phys. Res. **223** (1984) 166.

[Zie88] J.F. Ziegler & J.M. Manoyan, Nucl. Instr. and Meth. B **35** (1988) 215.